Simulated Arctic Ocean Response to Doubling of Riverine Carbon and Nutrient Delivery

Jens Terhaar, J.C. Orr, C. Ethé, P. Regnier, L Bopp

▶ **To cite this version:**

Jens Terhaar, J.C. Orr, C. Ethé, P. Regnier, L Bopp. Simulated Arctic Ocean Response to Doubling of Riverine Carbon and Nutrient Delivery. Global Biogeochemical Cycles, 2019, 33 (8), pp.1048-1070. 10.1029/2019GB006200 . hal-02974125

HAL Id: hal-02974125
https://hal.science/hal-02974125

Submitted on 28 Oct 2020

HAL is a multi-disciplinary open access archive for the deposit and dissemination of scientific research documents, whether they are published or not. The documents may come from teaching and research institutions in France or abroad, or from public or private research centers.

L'archive ouverte pluridisciplinaire **HAL**, est destinée au dépôt et à la diffusion de documents scientifiques de niveau recherche, publiés ou non, émanant des établissements d'enseignement et de recherche français ou étrangers, des laboratoires publics ou privés.

Global Biogeochemical Cycles

RESEARCH ARTICLE
10.1029/2019GB006200

Simulated Arctic Ocean Response to Doubling of Riverine Carbon and Nutrient Delivery

J. Terhaar[1,3], J. C. Orr[1], C. Ethé[2], P. Regnier[3], and L. Bopp[4]

[1]Laboratoire des Sciences du Climat et de l'Environnement, LSCE/IPSL, CEA-CNRS-UVSQ, Université Paris-Saclay, Paris, France, [2]Institut Pierre et Simon Laplace, Paris, France, [3]Biogeochemistry and Earth System Modelling, Department of Geoscience, Environment and Society, Université Libre de Bruxelles, Brussels, Belgium, [4]LMD/IPSL, Ecole Normale Supérieure / PSL Research University, CNRS, Ecole Polytechnique, Sorbonne Université, Paris, France

Key Points:
- Model sensitivity tests were used to quantify the response of Arctic Ocean biogeochemistry to changing river fluxes of carbon and nutrients
- Doubling riverine nutrient fluxes increase net primary production by 11% basinwide, 34–35% regionally, and 100% close to river mouths
- Ocean acidification is worsened by enhanced river fluxes of dissolved organic carbon but reduced by fluxes of inorganic carbon and alkalinity

Supporting Information:
- Supporting Information S1

Correspondence to:
J. Terhaar,
jens.terhaar@lsce.ipsl.fr

Citation:
Terhaar, J., Orr, J. C., Ethé, C., Regnier, P., & Bopp, L. (2019). Simulated Arctic Ocean response to doubling of riverine carbon and nutrient delivery. *Global Biogeochemical Cycles*, *33*, 1048–1070. https://doi.org/10.1029/2019GB006200

Received 25 FEB 2019
Accepted 22 JUL 2019
Accepted article online 29 JUL 2019
Published online 21 AUG 2019

©2019. The Authors.
This is an open access article under the terms of the Creative Commons Attribution License, which permits use, distribution and reproduction in any medium, provided the original work is properly cited.

Abstract The Arctic Ocean, more than any other ocean, is influenced by riverine input of carbon and nutrients. That riverine delivery is likely to change with climate change as runoff increases, permafrost thaws, and tree lines advance. But it is unknown to what extent these changes in riverine delivery will affect Arctic Ocean primary production, air-to-sea CO_2 fluxes, and acidification. To test their sensitivity to changing riverine delivery, we made sensitivity tests using an ocean circulation model coupled to an ocean biogeochemical model. In separate idealized simulations, riverine inputs of dissolved inorganic carbon (C_T), dissolved organic carbon (DOC), and nutrients were increased by 1%/year until doubling. Doubling riverine nutrient delivery increased primary production by 11% on average across the Arctic basin and by up to 34–35% locally. Doubling riverine DOC delivery resulted in 90% of that added carbon being lost to the atmosphere, partly because it was imposed that once delivered to the ocean, the riverine DOC is instantaneously remineralized to C_T. That additional outgassing, when considered alone, reduced the net ingassing of natural CO_2 into the Arctic Ocean by 25% while converting the Siberian shelf seas and the Beaufort Sea from net sinks to net sources of carbon to the atmosphere. The remaining 10% of DOC remained in the Arctic Ocean, but having been converted to C_T, it enhanced acidification. Conversely, doubling riverine C_T increased the Arctic Ocean's average surface pH by 0.02 because riverine total alkalinity delivery increased at the same rate as riverine C_T delivery.

1. Introduction

It is uncertain how river delivery of carbon and nutrients will change and how these changes will affect the coastal and open ocean (Regnier et al., 2013). The largest of these changes will occur in the Arctic Ocean into which 11% of the global river discharge drains (McClelland et al., 2012) even though it is the world's smallest ocean, representing only 4% of the global ocean area and 1% of its volume (Jakobsson, 2002).

Total Arctic river discharge has continued to increase since the beginning of the last century, for example, with outflow from the six largest Eurasian rivers draining into the Arctic Ocean growing by 7% from 1939 to 1999 (McClelland et al., 2004; Peterson et al., 2002). Between 1964 and 2000, river discharge from 16 Eurasian rivers that drain into the Arctic Ocean increased by 11% (McClelland et al., 2006). Conversely, the Canadian river discharge into the Arctic Ocean declined by 10% from 1964 to 2003 (Déry & Wood, 2005), although that was reversed during 1989 to 2007, a period that showed a 15% increase in river discharge (Déry et al., 2009). Further increases in Arctic river discharge are expected given projected future increases in precipitation (Peterson et al., 2002). More precisely, a 16–28% increase of freshwater discharge into the Arctic Ocean during the 21st century is projected by atmosphere-ocean general circulation models forced under the SRES A1, A2, and B1 scenarios (Lawrence & Slater, 2005; Nohara et al., 2006). Such increases would in turn affect Arctic Ocean circulation and biogeochemistry, for example, leading to increased stratification, decreased vertical mixing, decreased nutrient supply from deeper waters, decreased primary production, and enhanced acidification (Carmack et al., 2015).

Primary production and acidification are also affected by riverine delivery of carbon and nutrients (Semiletov et al., 2016; Tremblay et al., 2015). Out of all the dissolved inorganic carbon (C_T) that is delivered to the global ocean by rivers, 13% to 15% is delivered into the Arctic Ocean (Tank, Raymond, et al., 2012). In addition, the ocean delivery of dissolved organic carbon (DOC) from the six largest Arctic rivers is 2.5 times

larger than that from temperate rivers having similar watershed size and water discharge (Raymond et al., 2007). Riverine carbon and nutrient delivery influences Arctic Ocean biogeochemistry in multiple ways, for example, by increasing primary production due to riverine nutrient delivery (Letscher et al., 2013; Le Fouest et al., 2013, 2015, 2018), reducing CO_2 uptake over the Siberian shelf seas due to their large riverine DOC delivery (Anderson et al., 2009; Manizza et al., 2011), and enhancing coastal ocean acidification also due to DOC delivery (Semiletov et al., 2016).

Despite the substantial riverine delivery of carbon and nutrients to the Arctic Ocean and the associated potentially large impacts on its biogeochemistry, long-term measurements of ammonium and dissolved organic nitrogen (DON) fluxes in Russian rivers were found to be unreliable (Holmes et al., 2000, 2001). To establish a better database for riverine fluxes to the Arctic Ocean, the Pan-Arctic River Transport of Nutrients, Organic Matter, and Suspended Sediments project (PARTNERS) was launched in 2003 (McClelland et al., 2008). PARTNERS made time-coordinated measurements of nutrients and carbon throughout the year in the six largest Arctic rivers (Ob, Yenisei, Lena, Kolyma, Yukon, and Mackenzie), which cover a combined watershed area of 11.3×10^6 km^2 (55% of Arctic watersheds). In 2008, the measurement program of the PARTNERS project was continued via the Arctic Great Rivers Observatory (ArcticGRO).

These observational programs have advanced the ability to assess present-day Arctic riverine fluxes, but of course they do not tell us how those fluxes could change in the future nor the corresponding effects on the biogeochemistry of the Arctic Ocean. Future riverine fluxes of carbon and nutrients are likely to increase due to advancing tree lines (Harsch et al., 2009), deepening of the active permafrost layer (Oelke et al., 2004), and degrading permafrost. Near-surface permafrost is projected to decline from 10.5 to 1.0×10^6 km^2 by 2100 in a fully coupled global climate model (CCSM3) forced under the SRES A2 emission scenario (Lawrence & Slater, 2005), a trend that is expected to enhance riverine delivery of C_T (Tank, Frey, et al., 2012; Walvoord & Striegl, 2007) and total alkalinity (A_T) (Drake et al., 2018) to the Arctic Ocean. Simultaneously, there may be an associated 29–46% increase in DOC flux from peatlands, namely, from the West Siberian watersheds, based on the observed relationship between atmospheric temperature and riverine DOC concentrations and projected temperature increases under both the SRES A2 and B2 scenarios (Frey & Smith, 2005). Also projected for the same watersheds are simultaneous increases in concentrations of DON (32–53%), total dissolved nitrogen (30–50%), and total dissolved phosphorus (29–47%; Frey et al., 2007). Nevertheless, Frey and McClelland (2008) question these projected increases in inorganic nitrogen and organic matter delivery because of the large uncertainties associated with river discharge projections. Faced with uncertainties, scientists have used idealized forcing scenarios to characterize the response of complex systems. For example, Friedlingstein et al. (2001) used idealized simulations to describe the response of the land and ocean sinks to increasing atmospheric CO_2 and changing climate. That is, with a system that combines a coupled ocean-atmosphere general circulation model and models of the carbon cycle on land and in the ocean, they increased atmospheric CO_2 by 1%/year and assessed the amount of atmospheric CO_2 that was taken up by land and by ocean. The responses of these land and ocean sinks were then divided into those from increasing atmospheric CO_2 and from changing climate by making two different simulations. Likewise, Boer and Arora (2010) as well as Roy et al. (2011) calculated the same responses but with more plausible socioeconomic scenarios. Yet calculated climate sensitivities depend on the scenario, so there has been a return to using the classical 1%/year idealized increase scenario (Arora et al., 2013).

This same idealized approach could be transposed to assess sensitivities of how changes in atmospheric CO_2 and riverine input of carbon and nutrients, driven in part by climate change, will alter projected changes in ocean acidification (Steinacher et al., 2009; Steiner et al., 2013), air-to-sea CO_2 fluxes (Bates et al., 2006), ocean C_T (Anderson & Kaltin, 2001), and primary production (Vancoppenolle et al., 2013), all of which may directly or indirectly affect the marine ecosystem (Darnis et al., 2012; Riebesell et al., 2013). Quantifying such sensitivities would offer common ground from which to compare models and gauge their developments regarding how river fluxes affect Arctic Ocean biogeochemistry.

For example, models disagree on the sign of the change in primary production during the 21st century (Vancoppenolle et al., 2013). They also disagree among themselves concerning the extent of future shoaling of the deep aragonite saturation horizon (Steiner et al., 2013). Likewise, the sign of the future change in the air-to-sea CO_2 flux in the Arctic Ocean projected by models (Roy et al., 2011) is opposite that estimated by one observational study (Cai et al., 2010), while it agrees with another (Bates et al., 2006). Yet none of the model studies consider increases in the partial pressure of CO_2 (pCO_2) from changes in riverine DOC. Few earth

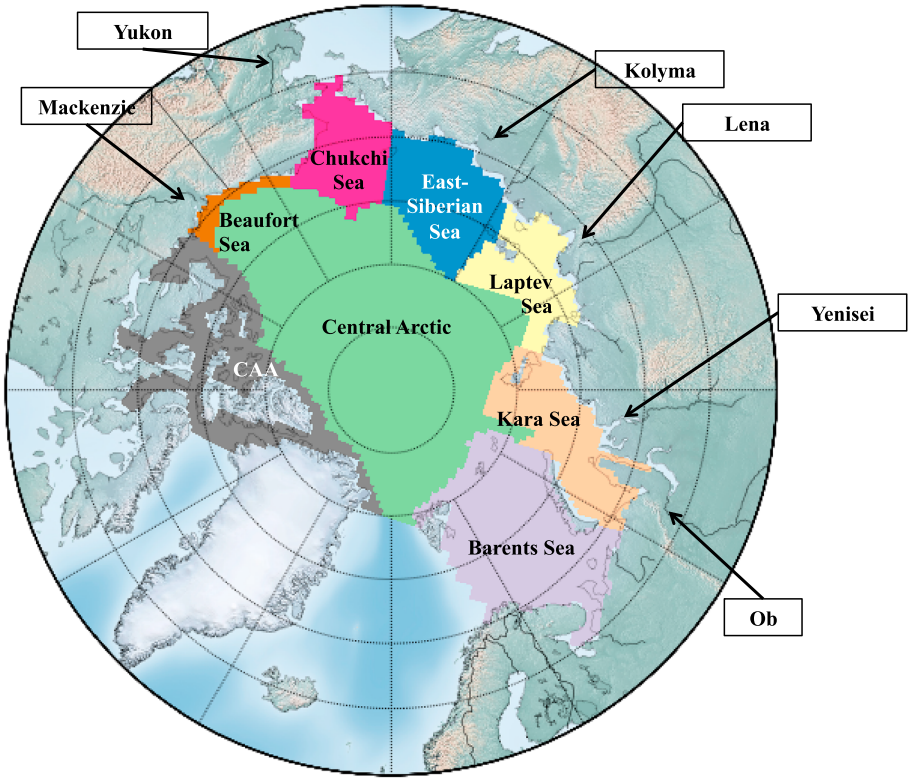

Figure 1. Arctic regional seas and its six major rivers, out of which all but the Yukon drain into the Arctic Ocean.

system models account for riverine input of carbon and nutrients. Those that do only do so in a rudimentary way even though observations indicate that such riverine input affects Arctic Ocean acidification (Chierici & Fransson, 2009; Semiletov et al., 2016), air-to-sea CO_2 fluxes (Cai et al., 2010; Manizza et al., 2011), and primary production (Le Fouest et al., 2015; Tank, Manizza, et al., 2012).

Our aim here is to assess how changes in riverine fluxes affect simulated biogeochemistry, in part by providing sensitivities that quantify the effects from changes in riverine delivery of carbon and nutrients and those from increasing atmospheric CO_2. For simplicity, this study neglects effects of climate change on Arctic Ocean biogeochemistry, such as warming, stratification, and sea ice melt.

2. Methods

2.1. Arctic Regions

To assess spatial patterns in how changes in riverine carbon and nutrient delivery affect its biogeochemistry, the Arctic Ocean is divided into eight regions (Figure 1). The Central Arctic includes all waters where the seafloor is deeper than 500 m. The remaining area is then divided into seven coastal seas, classed either as "exterior" (Barents Sea, Chukchi Sea, and Canadian Arctic Archipelago [CAA]) because of their direct exchange with the Atlantic or Pacific Ocean or "interior" (Kara Sea, Laptev Sea, East Siberian Sea, and Beaufort Sea) because they have no such exchange.

2.2. Coupled Ocean-Biogeochemical Model

This study relies on the ocean general circulation modeling platform Nucleus for European Modelling of the Ocean (NEMO), more specifically its version "v3.6 stable." Here we use the full NEMO system, consisting of the ocean general circulation model OPA (Madec, 2008), the Louvain-la-Neuve Sea Ice Model (LIM3.6) (Rousset et al., 2015), and the "Tracers in the Ocean Paradigm" (TOP) model. In our case, TOP couples NEMO-LIM to the biogeochemical model "Pelagic Interactions Scheme for Carbon and Ecosystem Studies" (PISCES-v2; Aumont et al., 2015).

Simulations were made with the same global configuration of NEMO known as ORCA1 (1° nominal horizontal resolution), having a normal Mercator grid south of 20°N but a distorted grid north of that boundary

to avoid the standard grid singularity at the North Pole (over ocean). Instead, that North Pole singularity is replaced for numerical efficiency by two grid singularities over land (over North America and over Eurasia; Madec & Imbard, 1996). That distortion also causes the model's horizontal resolution to be higher in the Arctic Ocean, where the horizontal grid length varies from 25 to 63 km. Vertically, the model is split into 75-depth levels whose thicknesses increase with depth from 1 m (level 1) to 204 m (level 74). The depth of the deepest cell (level 74) can reach up to 408 m, being extended into level 75 as a function of the bathymetry (partial steps; Barnier et al., 2006). Also, at other vertical levels, the partial steps approach allows the depth of the deepest grid cell to be variable and thus permits a better representation of the ocean bathymetry. The ORCA1 global bathymetry map is derived from three different sources: (1) the 2-min ETOPO2 bathymetry map from the National Geophysical Data Center, applied over most of the ocean (Smith & Sandwell, 1997), (2) the IBCAO bathymetric data, applied in the Arctic (Jakobsson et al., 2000), and (3) the BEDMAP bathymetric data, applied south of 72°S (Lythe & Vaughan, 2001). Because ORCA1 does not explicitly resolve ocean eddies, subgrid-scale eddy effects are parameterized by implementing the Gent and McWilliams (1990) scheme with an eddy diffusion coefficient of 1,000 m^2/s. The corresponding lateral diffusivity coefficient is 1,000 m^2/s, while its lateral viscosity coefficient is 2×10^4 m^2/s.

A detailed description of the biogeochemical model PISCES is provided by Aumont et al. (2015). Briefly, it simulates four plankton types (nanophytoplankton, diatoms, microzooplankton, and mesozooplankton) as well as the biogeochemical cycles of the main nutrients (N, P, Fe, and Si), C_T, A_T, and dissolved O_2. Its total net primary production (NPP) depends on temperature and is limited by light and nutrients. In PISCES, N, P, and Fe limit growth of all phytoplankton, while Si also limits growth of diatoms. For all plankton, the C:N:P molar ratio of organic matter is held constant at 122:16:1 (Takahashi et al., 1985), while the O_2:C molar ratio is fixed at 1.34 (Körtzinger et al., 2001). The same C:N:P ratio is also fixed for the PISCES nonliving compartments of marine semilabile dissolved organic matter as well as small and large sinking particles. The PISCES model explicitly simulates, as separate tracers, concentrations of phytoplankton chlorophyll, Fe, and Si (for diatoms only). The air-to-sea CO_2 flux in PISCES is calculated from the air-sea difference in the partial pressure of CO_2, wind speed, sea ice fraction, and CO_2 solubility and Schmidt number as summarized by Bourgeois et al. (2016). In PISCES, calcite is the only form of $CaCO_3$ that is explicitly simulated. It is transported as a passive tracer in the model and its internal sources and sinks are dissolution and precipitation. That "$CaCO_3$ concentration" is not used to compute the aragonite saturation state (Ω_{arag}), which would be erroneous. Rather, Ω_{arag} is calculated offline from $[Ca^{2+}]$ and $[CO_3^{2-}]$ concentrations using the routines from Orr and Epitalon (2015) with equilibrium constants recommended for best practices and simulated temperature, salinity, C_T, A_T, total dissolved silicon (Si_T), and total dissolved inorganic phosphorus (P_T).

2.3. River Input

At the beginning of all simulations, the river inputs into the Arctic Ocean are based on annual fluxes of terrigenous DOC, dissolved inorganic nitrogen (DIN), DON, P_T, dissolved organic phosphate (DOP), and Si_T from the Global NEWS 2 model (GN2; Mayorga et al., 2010) and C_T from the Global Erosion Model (GEM; Ludwig et al., 1998). The GN2 model is a composite of independent submodels for dissolved inorganic, dissolved organic, and particulate C, N, and P, as well as dissolved Si. The GN2 submodels for dissolved elements use a unified formulation. All GN2 submodels use hydrological and physical factors, hydrography, and basin characteristics to estimate annual riverine exports of DOC and nutrients. The GN2 submodels consider both natural processes and anthropogenic activities. GEM establishes a relationship between C_T yield and hydroclimatic and geomorphological factors for four different climatic zones in 60 different river basins. These relationships depend on the climatic zone and are then applied to all rivers around the world. In our simulations, lateral boundary conditions at river mouths are applied based on contemporary annual river fluxes from GEM's C_T (R_{C_T}) and GN2's DOC (R_{DOC}), DIN and DON (R_N), P_T and DOP (R_P), and Si (R_{Si}). Along with the corresponding freshwater discharge rates given with GEM and GN2, riverine concentrations of carbon and nutrients are calculated. These concentrations are then multiplied with the monthly river discharge from Dai and Trenberth (2002) used in NEMO. The resulting river fluxes are presented in Table 1.

For simplicity, in the ORCA1-PISCES model it is assumed that the riverine A_T:C_T ratio is 1.0. Conversely, the observed A_T:C_T ratio in rivers ranges from 0.6 in the Congo River (Wang et al., 2013) to 1.1 in the Delaware Estuary (Joesoef et al., 2017). In the Mississippi River, that ratio is 1.0 (Cai, 2003). For the six largest Arctic rivers, Tank, Raymond, et al. (2012) observed an average carbonate alkalinity (A_C):C_T ratio of 0.91 (0.72–0.94). Although they measured A_T, they report A_C, after subtracting the measured contribution from organic acids, assuming that alkalinity contributions from P_T and Si_T are negligible. Thus, their

Table 1
River-to-Ocean Fluxes of C_T Derived From GEM and of DOC and Nutrients Derived From GN2 Compared to Data-Based Estimates of R_{C_T}, R_{DOC}, R_N, R_P, and R_{Si} (Holmes et al., 2012; Manizza et al., 2009; Tank, Raymond, et al., 2012; section 3.1)

	R_{DOC} (Tg C/year)		R_{C_T} (Tg C/year)		R_N (Tg N/year)		R_P (Tg P/year)		R_{Si} (Tg Si/year)	
Region	Model	Data	Model	Data	Model	Data	Model	Data	Model	Data
Arctic Ocean	20.3	29.9	49.8	40.8	2.30		0.090		13.4	
Barents Sea	1.9	4.3	7.1	4.7	0.22		0.010		1.4	
Kara Sea	7.8	11.1	10.0	14.7	1.09		0.037		6.6	
Ob River	3.3	4.1	1.5	5.9	0.45	0.19	0.015	0.017	3.1	1.5
Yenisei River	2.9	4.6	5.0	7.0	0.43	0.16	0.015	0.010	2.0	1.7
Laptev Sea	4.0	8.3	18.5	8.2	0.42		0.020		1.8	
Lena River	2.6	5.7	4.7	5.8	0.24	0.17	0.013	0.006	1.1	1.3
East Siberian Sea	1.5	2.4	1.9	1.7	0.12		0.005		0.7	
Kolyma river	0.8	0.8	0.9	0.8	0.06	0.03	0.003	0.001	0.2	0.3
Chukchi Sea	0.6	0.4	1.1	1.0	0.05		0.002		0.5	
Beaufort Sea	2.4	2.5	7.9	7.6	0.16		0.007		1.4	
Mackenzie River	1.9	1.4	6.3	6.3	0.12	0.06	0.006	0.003	0.8	0.6
CAA	2.0	1.0	3.3	3.0	0.24		0.008		0.9	

Note. Fluxes into the Arctic Ocean and its regional seas are given as the cumulative amount draining into each region from all Arctic rivers. GEM = Global Erosion Model; DOC = dissolved organic carbon; CAA = Canadian Arctic Archipelago.

A_C is directly comparable to the simulated A_T in PISCES, which neglects organic acids. By using a globally constant A_T:C_T ratio of 1.0, we overestimate the riverine A_T flux (R_{A_T}) by 6–28% depending on the river.

PISCES also models the influence of R_{DOC} simplistically. In the standard version of PISCES, the imposed river flux of terrigenous DOC (R_{DOC}) is assumed to be extremely labile, being remineralized instantaneously, that is, it is added to the ocean in the form of already remineralized carbon (C_T; Aumont et al., 2015). That simplicity is maintained here, considering that as a first sensitivity assessment, our preference is to provide a limit rather than a best estimate for ocean behavior. Indeed, there are large uncertainties concerning the lability of terrigenous DOC. In North American rivers, Holmes et al. (2008) estimate that 20–40% of terrigenous DOC remineralizes within 3 months, whereas in Eurasian rivers Kaiser et al. (2017) estimate that close to 50% of terrigenous DOC remineralizes within a year. That partitioning may also change in the near future, as more old, labile terrestrial carbon becomes available due to thawing of permafrost (Vonk et al., 2013). Similarly, riverine fluxes of DON and DOP were added to the ocean as DIN and P_T.

Given our two simplifications, that is, that the riverine flux of A_T (R_{A_T}) equals R_{C_T} and that R_{DOC} is instantaneously converted to C_T as it is added to the ocean, the effective ratio $R^{\star}_{A_T}$:$R^{\star}_{C_T}$, imposed as the river flux boundary condition for PISCES, is

$$\frac{R^{\star}_{A_T}}{R^{\star}_{C_T}} = \frac{R_{C_T}}{R_{C_T} + R_{DOC}}, \tag{1}$$

where $R^{\star}_{C_T}$ and $R^{\star}_{A_T}$ are the river flux boundary conditions for PISCES calculated from the river fluxes derived from GEM (R_{C_T}) and Global NEWS 2 (R_{DOC}). Thus, an increase in R_{C_T} would increase the $R^{\star}_{A_T}$:$R^{\star}_{C_T}$ ratio, while an increase in R_{DOC} would reduce it. To illustrate the uncertainties associated with the two simplifications, we compared our calculated $R^{\star}_{A_T}$:$R^{\star}_{C_T}$ boundary condition for the five major rivers that drain directly into the Arctic Ocean to what it would have been had we used a more realistic R_{DOC} lability of 50% (Kaiser et al., 2017) and the R_{A_T}:R_{C_T} from Tank, Raymond, et al. (2012), which varies among those rivers (Figure S1 in the supporting information). Relative to our simplified case, an R_{DOC} lability of 50% would increase the $R^{\star}_{A_T}$:$R^{\star}_{C_T}$ ratio, while imposing a R_{A_T}:R_{C_T} below one, as observed, would reduce it. Combined, the two simplifications cause the $R^{\star}_{A_T}$:$R^{\star}_{C_T}$ ratio to be overestimated in the CTL simulation by 6% in the Kolyma River and to be underestimated by 5–22% in the remaining four rivers. Due to our two simplifications, the change

Table 2
Scheme of the Five Simulations for the Sequential 1%/year Increases in Atmospheric CO_2 and Riverine C_T, DOC, and Nutrient Fluxes

Simulation	CO_2^{atm}	R_{DOC}	R_{C_T}	R_{NUT}(N,P,Si)
CTL	-	-	-	-
CO_2	•	-	-	-
ROC	•	•	-	-
RIC	•	•	•	-
RUT	•	•	•	•

Note. DOC = dissolved organic carbon.

of the $R^{\star}_{A_T}$:$R^{\star}_{C_T}$ ratio when riverine DOC is doubled is underestimated by 7% for the Ob and overestimated by 26–55% in the remaining four rivers. However, our two simplifications do not alter the direction of the change in the $R^{\star}_{A_T}$:$R^{\star}_{C_T}$ ratio, as discussed in section 4.2. Invariably, that ratio declines when the riverine DOC flux is doubled, and it increases when the riverine C_T flux is doubled.

2.4. Transient Simulations

We made five 75-year simulations, each with the same physical forcing, the daily climatological DRAKKAR Forcing Set 4.4 (DFS4.4) (Brodeau et al., 2010). The DFS4.4 forcing includes historical reanalyses of atmospheric air temperature and humidity at 2 m, zonal and meridional wind fields at 10 m, downward shortwave and longwave radiation at 2 m, and the net surface freshwater flux (precipitation minus evaporation). The first version of DFS4.4 is based on the ERA40 reanalysis (Uppala et al., 2005) and covers 45 years (1958–2002). DFS4.4 was extended until 2012 using ERA-interim reanalysis (Dee et al., 2011) thus covering 55 years in total. For our 75-year simulations, after the first 55 years we reused the initial 20 years of DFS4.4. This relooping of DFS4.4 is facilitated by efforts made during its construction to make adjustments for global and regional biases and to reduce time discontinuities in data from different sources, which would otherwise result in spurious trends (Brodeau et al., 2010).

To quantify the effect of changes in riverine delivery on Arctic biogeochemistry, we separately altered one aspect of each of the simulations: (1) a preindustrial control simulation (CTL) with a constant atmospheric CO_2 fixed at 284.7 ppm (1850) having constant riverine input as prescribed in section 3.1; (2) a simulation just like CTL except that atmospheric CO_2 is increased by 1%/year (CO_2); (3) a simulation just like CO_2 except that R_{DOC} is also increased by 1%/year (ROC), which is instantaneously and completely remineralized as it enters the ocean, thus increasing $R^{\star}_{C_T}$; (4) a simulation just like ROC except that R_{C_T} is also increased by 1%/year (RIC), which increases $R^{\star}_{A_T}$ as well as $R^{\star}_{C_T}$; and (5) a simulation just like RIC except that the nutrient river flux (R_{NUT}) is also increased by 1%/year (RUT; Table 2). The 1%/year increase in riverine inputs concerns all rivers, not just those in the Arctic. That rate of increase leads to a doubling after 70 years. Taking differences between simulations allows us to distinguish the effects of increases in atmospheric CO_2, R_{DOC}, R_{C_T}, and R_{NUT} on Arctic Ocean biogeochemistry. These differences between simulations are referred to as ΔCO_2 (CO_2-CTL), ΔROC (ROC-CO_2), ΔRIC (RIC-ROC), and ΔRUT (RUT-RIC).

To smooth out interannual variations, all model results were compared in terms of their averages over simulated years 66–75, that is, centered around the time when the simulated atmospheric CO_2 doubled from the imposed 1%/year increase. To assess air-to-sea CO_2 fluxes, NPP, pH, and Ω_{arag}, we also calculated 10-year averages for years 26 to 35 when atmospheric CO_2 varies between 369 and 399 ppm, similar to values observed at the beginning of this century. Initial conditions for atmospheric CO_2 represent the preindustrial level, while those for river input and climate are based on modern data.

Simulated biogeochemical processes, such as the air-to-sea CO_2 flux and NPP, are affected by sea ice. Previous evaluation of the sea ice model component LIM3 coupled to the same ORCA1 configuration and forced by an updated version of the DRAKKAR Forcing Set 5.2 indicates that the simulated mean seasonal cycle and interannual variations of sea ice extent in the Arctic Ocean are much like those observed (Uotila et al., 2017). This simulated maximum sea ice extent in winter is ~7% larger than observed while minimum sea ice extent in summer generally agrees with observations.

Table 3
Sensitivity Factors Calculated for Ocean Carbon Storage, Cumulative Air-to-Sea CO_2 Flux, NPP, and pH in Response to an Increase of a Given Geochemical Forcing (atmospheric CO_2, Riverine DOC Flux, Riverine C_T Flux, and Riverine Nutrient Flux)

	Impact on			
Forcing	Carbon storage	Air-to-sea CO_2 flux	NPP	pH
Atmospheric CO_2	$\zeta_{\Delta CO_2}$ (4)	$\beta_{\Delta CO_2}$ (3)	-	$\xi_{\Delta CO_2}$ (12)
Riverine DOC flux	$\zeta_{\Delta ROC}$ (8)	$\beta_{\Delta ROC}$ (5)	-	$\xi_{\Delta ROC}$ (13)
Riverine C_T flux	$\zeta_{\Delta RIC}$ (9)	$\beta_{\Delta RIC}$ (6)	-	$\xi_{\Delta RIC}$ (14)
Riverine nutrient flux	$\zeta_{\Delta RUT}$ (10)	$\beta_{\Delta RUT}$ (7)	$\eta_{\Delta RUT}$ (11)	-

Note. Numbers in parentheses indicate the equations where these factors are defined in the text. NPP = net primary production; DOC = dissolved organic carbon.

2.5. Sensitivity Factors

Following the approach first proposed by Friedlingstein et al. (2003), we assessed the sensitivities of land and ocean carbon sinks to increasing atmospheric CO_2 and to anthropogenic climate change. This approach was extended here to calculate sensitivities of the Arctic Ocean carbon sink to the increasing riverine delivery of carbon and nutrients from rivers draining directly into the Arctic Ocean (R_{DOC}, R_{C_T}, and R_{NUT}; Table 3). Furthermore, these sensitivities were not only calculated for the ocean carbon storage and air-to-sea CO_2 flux but also for net primary production and pH.

To quantify the sensitivity of global ocean carbon storage to the atmospheric CO_2 increase ($\beta^{global}_{\Delta CO_2}$), our approach exactly follows that of Friedlingstein et al. (2006)

$$\beta^{global}_{\Delta CO_2} = \frac{\Delta C_O^{global}}{\Delta C_A} = \frac{\int \Delta F^{global} dt}{\Delta C_A}, \tag{2}$$

where ΔC_A is the change in the atmospheric CO_2 mixing ratio (ppm) between the beginning and end of the simulation, ΔC_O^{global} is the change of C_T in the global ocean during the same period, and ΔF^{global} is the difference in global air-to-sea CO_2 flux in response to increasing atmospheric CO_2. At the global scale, the time-integrated air-to-sea CO_2 flux and the change in carbon storage are identical. Regionally though, they are unlikely to be the same. In the Arctic Ocean, much of the anthropogenic carbon enters laterally (Terhaar et al., 2019a), causing these two diagnostics to differ. To distinguish between them in the Arctic Ocean, β is used to indicate the sensitivity of the air-to-sea CO_2 flux (equation (3)), while ζ is used for the sensitivity of ocean carbon storage

$$\beta_{\Delta CO_2} = \frac{\int \Delta F^{CO_2} dt}{\Delta C_A}, \tag{3}$$

$$\zeta_{\Delta CO_2} = \frac{\Delta C_O^{CO_2}}{\Delta C_A}, \tag{4}$$

where ΔF^{CO_2} is the difference in air-to-sea CO_2 flux in response to increasing atmospheric CO_2 areally integrated over the Arctic Ocean and $\Delta C_O^{CO_2}$ is the change in C_T storage within the Arctic Ocean in response to an increase in atmospheric CO_2.

Likewise, the sensitivities of the air-to-sea CO_2 flux to changes in R_{DOC}, R_{C_T}, and R_{NUT} are as follows:

$$\beta_{\Delta ROC} = \frac{\int \Delta F^{ROC} dt}{\int \Delta R_{DOC} dt}, \tag{5}$$

$$\beta_{\Delta RIC} = \frac{\int \Delta F^{RIC} dt}{\int \Delta R_{C_T} dt}, \text{ and} \tag{6}$$

$$\beta_{\Delta RUT} = \frac{\int \Delta F^{RUT} dt}{\int \Delta R_{NUT} dt}, \tag{7}$$

where ΔR_{DOC}, ΔR_{C_T}, and ΔR_{NUT} are differences of riverine input of each of those species into the Arctic Ocean between a given year and that at the beginning of each simulation, while ΔF^{ROC}, ΔF^{RIC}, and ΔF^{RUT} are the differences in air-to-sea CO_2 fluxes in response to increases in R_{DOC}, R_{C_T}, and R_{NUT} between the same two times after integrating areally over the Arctic Ocean. Similarly, the sensitivities of Arctic Ocean carbon storage to increasing riverine inputs of DOC, C_T, and nutrients are defined as

$$\zeta_{\Delta\mathrm{ROC}} = \frac{\Delta C_O^{\mathrm{ROC}}}{\int \Delta R_{\mathrm{DOC}} \mathrm{d}t}, \tag{8}$$

$$\zeta_{\Delta\mathrm{RIC}} = \frac{\Delta C_O^{\mathrm{RIC}}}{\int \Delta R_{C_T} \mathrm{d}t}, \text{ and} \tag{9}$$

$$\zeta_{\Delta\mathrm{RUT}} = \frac{\Delta C_O^{\mathrm{RUT}}}{\int \Delta R_{\mathrm{NUT}} \mathrm{d}t}, \tag{10}$$

where $\Delta C_O^{\mathrm{ROC}}$, $\Delta C_O^{\mathrm{RIC}}$, and $\Delta C_O^{\mathrm{RUT}}$ are the time differences in Arctic Ocean C_T, integrated vertically and areally over the Arctic, induced by the corresponding increases in riverine input. The $\zeta_{\Delta\mathrm{RUT}}$ does not account for ocean POC and organic carbon burial.

It follows that the sensitivity of NPP (η) to changes in riverine nutrients is

$$\eta_{\Delta\mathrm{RUT}} = \frac{\int \Delta\mathrm{NPP}^{\mathrm{RUT}} \mathrm{d}t}{\int \Delta R_{\mathrm{NUT}}(t) \mathrm{d}t}, \tag{11}$$

where $\Delta\mathrm{NPP}^{\mathrm{RUT}}$ is the change in the vertically and horizontally integrated primary production from increased riverine nutrients. In the same way, sensitivities of pH (ξ) to changes in atmospheric CO_2 and inputs of riverine DOC and C_T are

$$\xi_{\Delta\mathrm{CO_2}} = \frac{\Delta pH^{\mathrm{CO_2}}}{\Delta C_A}, \tag{12}$$

$$\xi_{\Delta\mathrm{ROC}} = \frac{\Delta pH^{\mathrm{ROC}}}{\int \Delta R_{\mathrm{DOC}} \mathrm{d}t}, \text{ and} \tag{13}$$

$$\xi_{\Delta_{\mathrm{RIC}}} = \frac{\Delta pH^{\mathrm{RIC}}}{\int \Delta R_{C_T} \mathrm{d}t}, \tag{14}$$

where $\Delta\mathrm{pH}^{\mathrm{CO_2}}$, ΔpH^{ROC}, and $\Delta\mathrm{pH}^{\mathrm{RIC}}$ are the areally averaged changes in surface pH in response to increases in atmospheric CO_2, river input of DOC, and river input of C_T, respectively. To calculate these basinwide differences, the pH values at every grid cell in the Arctic Ocean were first converted to hydrogen ion concentrations $[H^+]$ on the total scale. The $[H^+]$ was then areally averaged at each time; the results were converted back to pH units, and the difference between the two simulations was taken.

3. Evaluation

3.1. Riverine Forcing

To evaluate the Arctic river flux estimates derived from GN2 and GEM, they were compared to data-based fluxes from the five largest Arctic rivers that drain directly into the Arctic Ocean (Table 1), that is, R_{C_T} is from Tank, Raymond, et al. (2012), R_{DOC} from Holmes et al. (2012) and Manizza et al. (2009), and R_{NUT} from Holmes et al. (2012). The model's GEM-derived total R_{C_T} flux to our Arctic Ocean domain (50 Tg C/year) falls within the uncertainty range of Tank, Raymond, et al. 2012's data-based estimate (41 ± 10 Tg C/year) from their extrapolation of the fluxes from the six major Arctic rivers to all rivers that discharge into the Arctic Ocean. The GEM-derived R_{C_T} fluxes typically overestimate the extrapolated fluxes but by no more than 12% in the East Siberian Sea, East Siberian Sea, the Chukchi Sea, the Beaufort Sea, and the CAA. Larger overestimates are found for the Barents Sea (+51%) and the Laptev Sea (+126%), while the general tendency is reversed in the Kara Sea (−32%).

The model's GN2-derived total R_{DOC} flux to our Arctic Ocean domain (20.3 Tg C/year) is 32% smaller than the data-based estimate (Manizza et al., 2009). The largest differences are located in the Barents Sea and

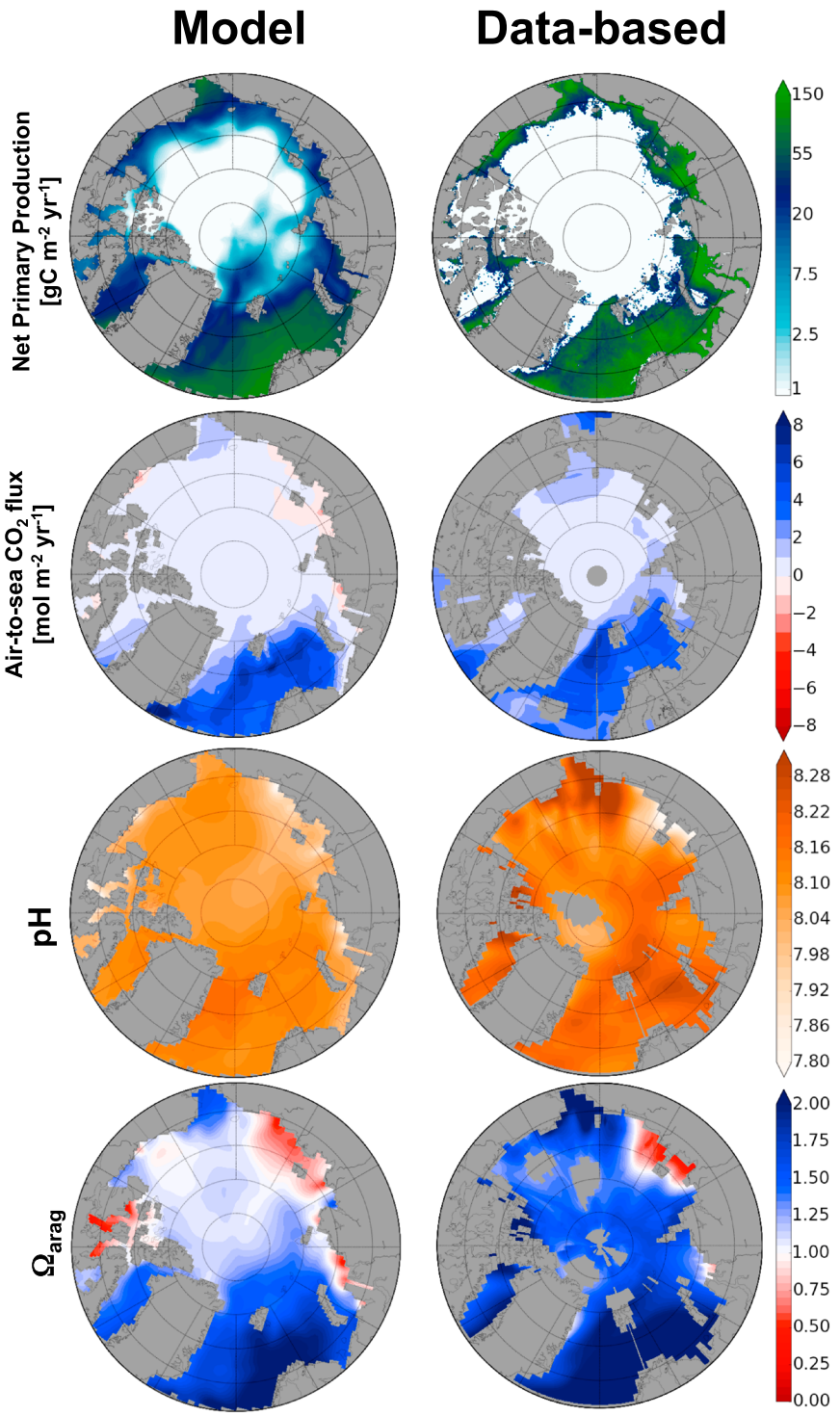

Figure 2. Simulated (left column) and data-based (right column) net primary production (NPP; integrated vertically), air-to-sea CO_2 flux, and surface pH and Ω_{arag} (top to bottom). Data-based depth-integrated NPP is derived from remotely sensed ocean color from SeaWiFS over 1998–2005 (Arrigo & van Dijken, 2011). The data-based, annual mean air-to-sea fluxes of total CO_2 from 1997 to 2013 are estimates derived with self-organizing pCO_2 maps (Yasunaka et al., 2016). Data-based surface pH and Ω_{arag} are from the GLODAPv2 gridded data product that normalizes observations to 2002 (Lauvset et al., 2016). The modeled air-to-sea CO_2 flux is the decadal average over years 26–35, over which the average atmospheric CO_2 was similar to that during the time span of the data-based estimates. The modeled pH and Ω_{arag} are averaged over July, August, and September to compare with the summer-biased GLODAPv2 data in the Arctic; conversely, the simulated air-to-sea CO_2 fluxes and NPP are annual average conditions as are the data-based estimates.

Table 4
Simulated NPP (CTL), Data-Based NPP, and Changes in NPP From ΔRUT at Doubling, All in Teragram of Carbon per Year

	CTL	Data-based[a]	ΔRUT
Arctic Ocean	164.7	432.9	18.0
Barents Sea	80.0	212.0	4.8
Kara Sea	21.8	16.0	4.4
Laptev Sea	7.3	21.9[b]	2.5
East Siberian Sea	6.2		1.6
Chukchi Sea	22.6	85.5	0.4
Beaufort Sea	3.4	2.3	1.2
CAA	9.3	93.0[c]	2.1
Central Arctic	14.1	2.2	1.0

Note. NPP = net primary production; CAA = Canadian Arctic Archipelago. [a]Hill et al. (2013). [b]In the data-based estimates, the Laptev and East Siberian Seas are only reported as a combined estimate. [c]In the data-based estimate, the CAA extends further south (to the Davis Strait) than in our study.

Laptev Sea, where the model's R_{DOC} fluxes are 52–56% smaller than the data-based estimates. The model's underestimated R_{DOC} flux into the Laptev Sea is largely caused by the underestimated GN2-based R_{DOC} flux from the Lena River that is 55% smaller than the data-based estimate. Furthermore, R_{DOC} fluxes for the Ob and Yenisei are 20–37% smaller, while those for the Kolyma agree with the data-based estimates. Unlike for those Siberian rivers, the GN2-based R_{DOC} flux for Canada's Mackenzie River is 36% larger than the data-based estimate.

For R_{NUT}, data-based fluxes have not been extrapolated to all Arctic rivers. They are available only for the five largest rivers draining directly into the Arctic Ocean (Holmes et al., 2012). For R_N, the GN2-based flux for the five observed rivers is 41–169% larger than data-based estimates. For R_P, the GN2-based flux estimates for the Yenisei, Lena, Kolyma, and Mackenzie are 50–200% larger than data-based estimates, while that for the Ob is 12% smaller. For R_{Si}, the GN2-based estimates for the Lena and Kolyma Rivers are 15–33% smaller than data-based estimates, while those for the Ob, Yenisei, and Mackenzie Rivers are 18–107% larger.

3.2. NPP

Simulated NPP from the CTL simulation was compared to the data product from Hill et al. (2013) derived from remotely sensed ocean color and observed vertical profiles of in situ chlorophyll *a*. From this data product, the estimated annual mean NPP, integrated vertically and areally over the Arctic Ocean, is 433 Tg C/year. The simulated NPP is much less (165 Tg C/year) but captures similar regional patterns (Figure 2 and Table 4).

Regionally, the largest model-data differences are found in the three exterior shelf seas: out of the basin-wide integrated bias, 49% (132 Tg C/year) is located in the Barents Sea, 31% (84 Tg C/year) in the CAA, and 24% (63 Tg C/year) in the Chukchi Sea (Table 4). The Barents Sea is strongly influenced by inflow from the adjacent Atlantic Ocean while the Chukchi Sea is influenced by inflow from the adjacent Pacific Ocean. Inflow of nutrients from those neighboring oceans fuels at least 20% of the Arctic Ocean NPP (Popova et al., 2013). That nutrient inflow may well be underestimated in the coarse-resolution model used here (ORCA1). Lateral water fluxes into the Arctic Ocean are underestimated using a coarser-resolution version (ORCA2) of the same NEMO-PISCES model, and they are improved when using higher-resolution eddying versions ORCA05 and ORCA025 (Terhaar et al., 2019a). Thus, our weak modeled lateral nutrient inflow may result in the low simulated NPP in the Barents Sea and Chukchi Sea. In the CAA, the discrepancy appears to be mainly caused by differences in the definition of the regional borders of the CAA, which is defined here to be bounded on the south by the Baffin Bay, but for Hill et al. (2013) it extends further south to the Davis Strait. The latter domain includes additional ice-free areas with strong primary production. Unlike for these exterior seas, the integrated simulated NPP in the interior seas is 4% (2 Tg C/year) smaller than the data-based estimates. The total underestimation in these exterior and interior seas adds up to more than 100% of the total bias, because the latter is reduced by an overestimation of simulated NPP in the Central Arctic by 540% (12 Tg C/year).

Table 5
Simulated Total Air-to-Sea CO_2 Fluxes (Tg C/year) for the CTL Simulation, the CO_2 Simulation at 379 ppm, and the Data-Based Estimates, as Well as the Differences Between Simulations

Region	CTL	ΔCO_2	ΔROC	ΔRIC	ΔRUT	CO_2	Data-based[a]
Arctic Ocean	69.1	19.3	−18.2	−2.1	5.4	91.6	65–199
Barents Sea	51.8	14.0	−2.1	−0.3	1.9	68.1	44–77
Kara Sea	4.9	−0.8	−6.1	−0.2	1.2	5.5	1–6
Laptev Sea	−1.0	−0.1	−3.6	−0.6	0.7	−1.0	1–4
East Siberian Sea	1.0	−0.1	−1.5	−0.1	0.4	1.2	0–13
Chukchi Sea	5.4	1.8	−0.5	−0.1	0.1	6.8	11–53
Beaufort Sea	−0.3	0.0	−1.6	−0.2	0.4	−0.2	2–3
CAA	1.3	1.5	−1.6	−0.2	0.6	2.5	16–24[b]
Central Arctic	6.0	3.0	−1.3	−0.4	0.3	8.9	6–19

Note. CAA = Canadian Arctic Archipelago.
[a]Bates and Mathis (2009). [b]Scaled to the area of the CAA assuming the same flux rate as in the Beaufort Sea.

Although most of the difference between simulated and data-based NPP may well be caused by model shortcomings, estimating NPP from remotely sensed ocean color remains challenging in the Arctic Ocean because of the large amount of colored dissolved organic matter, which is difficult to distinguish from chlorophyll *a* (Matsuoka et al., 2011). Therefore, part of the discrepancy between data-based and simulated NPP could also originate from observational artifacts.

3.3. Total Air-to-Sea CO_2 Flux

At present, all subregions of the Arctic Ocean take up both natural and anthropogenic carbon from the atmosphere. Eventually, most of that absorbed carbon is transported out of Arctic Ocean laterally (Bates & Mathis, 2009; Yasunaka et al., 2016), although some local outgassing is observed in the Pacific dominated sectors immediately after sea ice retreat in spring (Arrigo et al., 2010) and on the Siberian shelf in summer after high river discharge of terrigenous DOC (Anderson et al., 2009). The annually average total air-to-sea CO_2 flux in the Arctic Ocean is estimated to be 66–199 Tg C/year over 2000–2009 (Bates & Mathis, 2009). The simulated Arctic Ocean air-to-sea CO_2 flux at the same level of atmospheric CO_2 is 92 Tg C/year falling within the data-based range (Table 5). Three fourths of that air-to-sea CO_2 flux occurs in the Barents Sea. The next largest simulated air-to-sea CO_2 flux occurs in the Chukchi Sea but is 10 times smaller. The same regional pattern is displayed by data-based estimates with the Barents Sea absorbing 44–77 Tg C/year and the Chukchi Sea taking up 11–53 Tg C/year. This underestimation of the total air-to-sea CO_2 flux in the Chukchi Sea is consistent with the same region's underestimated NPP (Table 4).

3.4. Carbonate Chemistry

We evaluate the simulated surface ocean pH by comparing preindustrial, present-day, and future pH estimates to the simulated pH at the corresponding atmospheric CO_2 levels in the CO_2 simulation. Our simulated preindustrial surface pH averaged over the Arctic Ocean is 8.17, which is 0.06 less than that from a previous study with a coupled carbon-climate model (Steinacher et al., 2009).

When doubling atmospheric CO_2 in our model (569 ppm), average surface ocean pH decreases by 0.3. One third of this decrease occurs by the time that the model's atmospheric CO_2 reaches 347–379 ppm (equivalent to observed values over 1986–2005). The 0.1 decrease in pH when atmospheric CO_2 reaches 347–379 ppm agrees with the data-based estimate for that historical surface pH change for the Arctic Ocean (Anderson et al., 2010). The further 0.2 pH reduction by the time of atmospheric CO_2 doubling agrees with the projected decrease for Arctic Ocean surface pH calculated by an ensemble of CMIP5 models forced under the RCP4.5 scenario (Steiner et al., 2013), where atmospheric CO_2 reached 583 ppm 2100.

The simulated mean Arctic surface pH averaged over years 26–35, when the atmospheric CO_2 forcing averages 374 ppm, was further compared to the gridded GLODAPv2 climatology (Lauvset et al., 2016). Although the simulated surface pH is on average 0.01 too high, the model and data product both indicate notably lower pH in regions with high freshwater input (on the East Siberian shelf, along the transpolar drift, and near the mouths of the Ob and Yenisei Rivers) and higher pH along the east coast of Greenland, in the Kara Sea,

Table 6
Modeled Average Surface pH and Ω_{arag} for CTL and the Differences Between Simulations

Region	CTL	ΔCO_2	ΔROC	ΔRIC
		pH		
Arctic Ocean	8.17	−0.30	−0.02	0.02
Barents Sea	8.22	−0.30	0.00	0.01
Kara Sea	8.15	−0.32	−0.04	0.02
Laptev Sea	8.10	−0.29	−0.05	0.06
East Siberian Sea	8.13	−0.30	−0.02	0.02
Chukchi Sea	8.20	−0.30	0.00	0.01
Beaufort Sea	8.10	−0.27	−0.08	0.04
CAA	8.16	−0.28	−0.03	0.02
Central Arctic	8.18	−0.29	−0.01	0.01
		Ω_{arag}		
Arctic Ocean	1.53	−0.71	−0.02	0.06
Barents Sea	2.01	−0.93	0.00	0.02
Kara Sea	1.44	−0.70	−0.03	0.06
Laptev Sea	1.17	−0.55	−0.06	0.19
East Siberian Sea	1.17	−0.57	−0.02	0.06
Chukchi Sea	1.66	−0.78	−0.01	0.02
Beaufort Sea	1.29	−0.58	−0.09	0.11
CAA	1.38	−0.63	−0.04	0.05
Central Arctic	1.50	−0.69	−0.02	0.05

Note. CAA = Canadian Arctic Archipelago.

and near the St. Anna trough (Figure 2). Besides model deficiencies, differences between the model and the data-based product might be caused by the relatively sparse observations in space and time.

Regional averages of simulated preindustrial Ω_{arag} are all supersaturated (Table 6), consistent with other studies (Anderson et al., 2010; Steinacher et al., 2009), but are spatially heterogeneous, varying from 1.17 to 2.01. The regions corresponding to the largest values of Ω_{arag} are those that are strongly influenced by outside inflow, that is, the Barents Sea (Ω_{arag} = 2.01) adjacent to the Atlantic and the Chukchi Sea (Ω_{arag} = 1.66) adjacent to the Pacific. The regions corresponding to low values of Ω_{arag} are more influenced by riverine input, for example, the Laptev Sea (Ω_{arag} = 1.17) and the East Siberian Sea (Ω_{arag} = 1.17) (Table 6). The simulated spatial patterns in Ω_{arag} are similar to those found in the GLODAPv2 gridded data product (Lauvset et al., 2016; Figure 2) as well as in several other observational studies, all of which indicate near-zero Ω_{arag} values near the mouths of the Mackenzie (Chierici & Fransson, 2009), Yukon (Mathis et al., 2011), and Lena Rivers (Semiletov et al., 2016).

The low Ω_{arag} in the coastal Arctic Ocean is driven by the dilution from Arctic river waters, with not only relatively low A_T:C_T ratios (0.7–0.9) but also low A_T (500–1,600 μmol/kg) and C_T (650–1,700 μmol/kg; Tank, Raymond, et al. 2012). Typical open ocean values are higher for the A_T:C_T ratio (1.1–1.2) and for both A_T (2,300 μmol/kg) and C_T (2,150 μmol/kg). Out of the five major rivers that drain into the Arctic Ocean, it is the Kolyma River that exhibits the lowest A_T and C_T (500–1,000 μmol/kg) concentrations and the lowest A_T:C_T ratio (0.73), perhaps because of rapid degradation of large amounts of labile terrigenous DOC originating from the Arctic's largest watershed that is entirely covered by permafrost (Mann et al., 2015).

4. Changes Due to Increasing Riverine Input

4.1. Effect of Riverine Nutrient Increase

Doubling R_{NUT} increases the simulated NPP in the Arctic Ocean by 11% (18 Tg C/year; Table 4). That increase in NPP is equivalent to a consumption of 2.36 Tg N/year, about the same as the additional supply of riverine nitrogen to the Arctic Ocean (2.30 Tg N/year). Regionally, the largest absolute increases in NPP are simulated in the Barents Sea (+4.8 Tg C/year, i.e., +6%) and the Kara Sea (+4.4 Tg C/year, i.e., +20%; Table 4). The

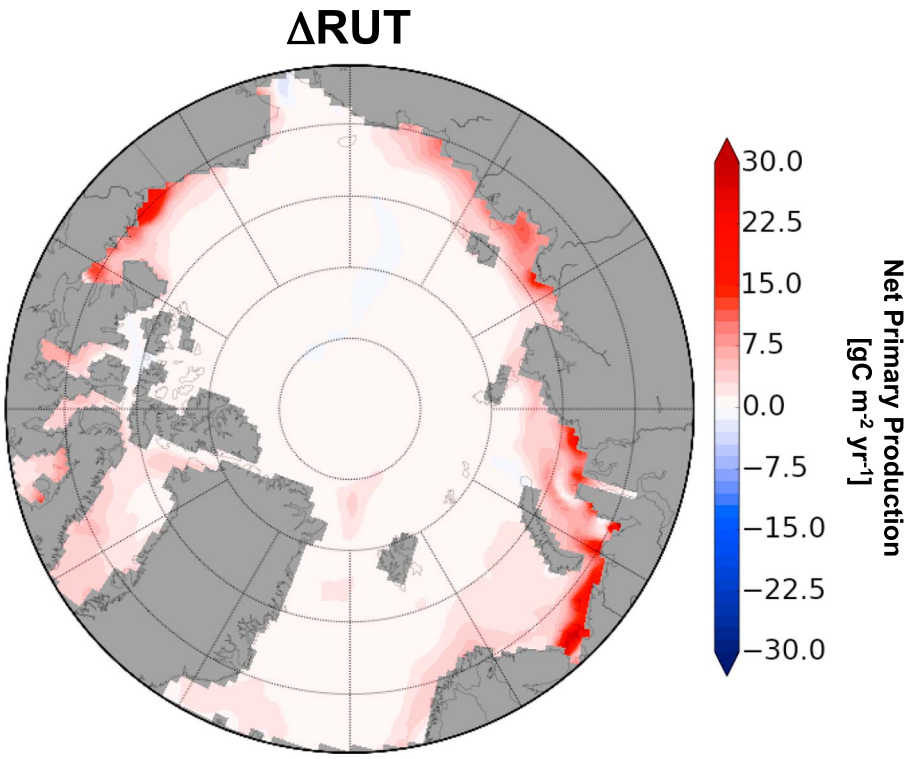

Figure 3. Simulated changes in depth-integrated net primary production (gC m^{-2}·year) from the doubling of riverine nutrients (ΔRUT).

large increase in the Barents Sea represents 27% of total Arctic NPP increase, although the increase in the R_{NUT} boundary condition represents only 10% of the total Arctic R_{NUT} increase (Table 1). This discrepancy suggests that region's increase in NPP is mainly driven by the additional influx of nutrients from outside the Arctic, given that the imposed R_{NUT} boundary condition increases in all rivers across the globe. The large increase in the Kara Sea represents 24% of the total Arctic NPP increase. As opposed to the Barents Sea, the increase of R_{NUT} into the Kara Sea is 47% of the total Arctic R_{NUT} increase. This large amount of extra nutrients thus solely explains Kara Sea's strong increase in NPP. Although the largest absolute changes in NPP occur in the Barents and Kara Seas, the largest relative changes occur in the Laptev and Beaufort Seas (+34% and +35%, respectively; Table 4).

Basinwide, the largest absolute changes in NPP are typically found within 100–200 km of the coastline, where they are often twice as large as average changes in adjacent waters further offshore (Figure 3). Yet the coastal-to-open ocean gradients in NPP may well be overestimated because in our simulations it is imposed that DON and DOP river fluxes (R_N and R_P) are instantaneously transformed into inorganic N and P as they enter the Arctic Ocean (section 3.1). In the real ocean, portions of the DON and DOP are transported offshore before being transformed into inorganic N and P, thus reducing the coastal-to-open ocean gradients in inorganic nutrients and NPP. Changes in NPP from the doubling of atmospheric CO_2, R_{C_T}, and R_{DOC} are generally more than a hundred times smaller than changes induced by doubling R_{NUT}. Indeed, the version of PISCES used here does not account for any direct effect of increasing C_T on phytoplankton productivity. The only indirect effects of changes in C_T on phytoplankton productivity are those involving carbonate dissolution and its implications on iron scavenging.

The simulated increase in NPP from the increase in R_{NUT} may be put into context by comparing it to NPP changes from climate-related reductions in sea ice projected by an ensemble of 11 CMIP5 models (Vancoppenolle et al., 2013). When these models were forced under the RCP8.5 scenario, the projected changes in Arctic Ocean NPP ranged from −110 to 253 Tg N/year for the average over 2080–2099 minus that over 1980–1999. Over that period, their average increase (58 Tg C/year) from climate change is around 3 times larger than the Arctic's basinwide increase due to the doubling of nutrient delivery in our RUT simulation.

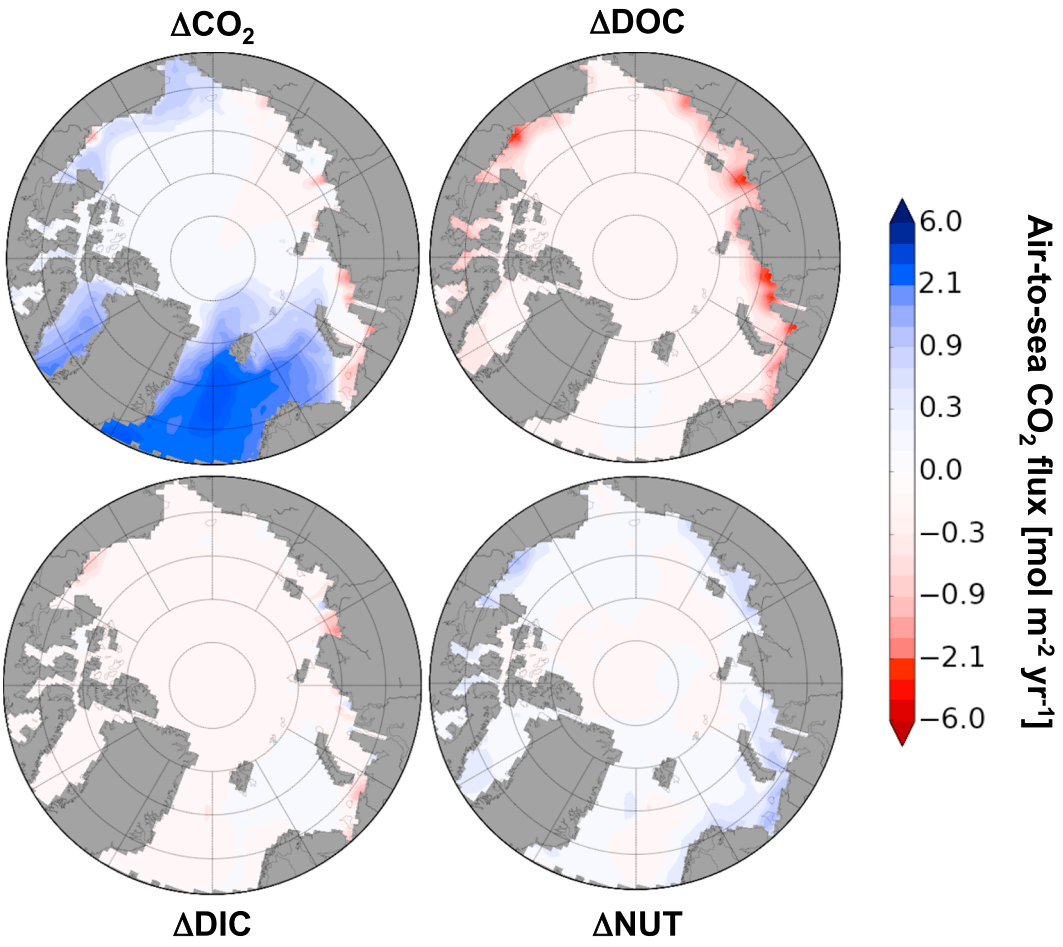

Figure 4. Modeled changes in air-to-sea CO_2 flux (mol· m^{-2}·year) for ΔCO_2, ΔROC, ΔRIC, and ΔRUT. The color bar axis is not regular.

The NPP increase from increased river nutrient fluxes also reduces surface C_T and thus surface ocean pCO_2, consequently enhancing the Arctic Ocean's air-to-sea CO_2 flux. The regions with the largest simulated increase in NPP (Barents Sea, Kara Sea, Laptev Sea, and the CAA; Table 4) also have the largest increase in the air-to-sea CO_2 flux (>0.6 Tg C/year for each) at year 70 (Table 5). These ties between NPP and air-to-sea CO_2 flux are similar to those seen in the other regional seas (Figures 3 and 4). At the time of R_{NUT} doubling, the change in NPP (18 Tg C/year) enhances the air-to-sea CO_2 flux and hence the Arctic Ocean's carbon storage by 1.83 Tg C/year of which 74% is stored in the Central Arctic Ocean, 11% in the CAA, and 6% in the Barents Sea. The remaining 7% is spread over the other Arctic shelf seas.

4.2. Effect of Riverine Carbon Increase

The simulated doubling of R_{DOC} reduces the net Arctic Ocean air-to-sea CO_2 flux by 18.2 Tg C/year, compensating 94% of the increase in the Arctic Ocean's air-to-sea CO_2 flux from the doubling of atmospheric CO_2 (Table 5). However, even if the air-to-sea CO_2 flux from the doubling of atmospheric CO_2 was completely compensated by R_{DOC}, the Arctic Ocean would still remain a sink of anthropogenic carbon, which mainly enters the Arctic Ocean laterally from the adjacent ocean basins (Olsen et al., 2015; Terhaar et al., 2019a).

Out of the added R_{DOC}, which is instantaneously converted to C_T, 90% is lost from the Arctic Ocean via outgassing of CO_2, 7% is transported out of the Arctic Ocean laterally, and 3% remains there. That outgassing is strongest in the Kara Sea (6.1 Tg C/year), which changes from a net sink to a net source of CO_2 (Table 5). The same change from CO_2 sink to source occurs in the East Siberian Sea. Although the Laptev and Beaufort Seas already exhibit outgassing at the end of the CO_2 simulation, the doubling of R_{DOC} increases that outgassing by up to several times. Thus, when R_{DOC}, is doubled, all interior Arctic shelf seas become sources of

carbon to the atmosphere even when atmospheric CO_2 levels have also doubled. Nevertheless, the Barents Sea, the Chukchi Sea, and the Arctic Ocean as a whole remain as sinks of atmospheric CO_2.

When R_{DOC} is doubled, the shelf waters immediately adjacent to large river mouths become small hot spots of CO_2 outgassing with intensities that are roughly 2 to 4 times as strong as associated outgassing from each surrounding regional sea (Figure 4). Away from river mouths, the associated outgassing declines rapidly as river waters are diluted in the sea and surface ocean pCO_2 plummets.

The assumption that the R_{DOC} boundary flux for PISCES is instantaneously converted to a flux of C_T as it enters the Arctic Ocean is merely a first limiting case for this idealized case study; it is much simpler than what occurs in the real world. From observed concentration gradients of terrigenous DOC in the Beaufort Gyre, Hansell et al. (2004) estimate that the half-life of terrigenous DOC in the Arctic Ocean is 7.1 ± 3.0 year, assuming exponential degradation and average residence time of river waters in the Arctic Ocean of 11 to 15 years based on isotopic water mass tracers. Hansell et al. (2004) further estimate that 21–32% of R_{DOC} is exported laterally to the North Atlantic before being remineralized to C_T in the Arctic. More recent studies suggest larger uncertainties, that is, that 20–50% of terrigenous DOC is remineralized in estuaries or the shelf seas (Holmes et al., 2008; Kaiser et al., 2017; Letscher et al., 2011; Spencer et al., 2009). Besides those large uncertainties, the future rate of degradation of terrestrial carbon may increase as old, terrestrial DOC, which is more labile, is mobilized during continuous thawing of permafrost (Holmes et al., 2008; Letscher et al., 2011; Vonk et al., 2013).

The model assumption that R_{DOC} is added to PISCES as C_T, equivalent to an instantaneous remineralization of terrigenous DOC at the river mouth, allows only 7% of that carbon to leave the Arctic (in the form of C_T), a smaller amount than estimated by Hansell et al. (2004), especially because their estimate does not consider the outflow of C_T from remineralized terrigenous DOC. That comparison further emphasizes that our model overestimates the loss of terrigenous DOC to the atmosphere and underestimates the export of that dissolved carbon out of the Arctic. Specifying a semilabile pool of terrigenous DOC in the model would lead to greater offshore transport of DOC before it could be remineralized to C_T. Consequently surface ocean pCO_2 and hence CO_2 outgassing would decrease near the river mouths and increase pCO_2 elsewhere in the Arctic Ocean as this semilabile terrigenous DOC would be remineralized later.

On the other hand, the GN2-based estimate for R_{DOC} used as a model boundary condition underestimates the data-based estimate by 32% (Table 1). If the model-imposed R_{DOC} had been larger, the outgassing of CO_2 to the atmosphere from doubling R_{DOC} would also have been larger. Therefore, the model's low R_{DOC} boundary condition compensates to some extent its overestimate of the loss of terrigenous DOC to the atmosphere caused by the direct remineralization of R_{DOC}.

Unlike the effect from a doubling of R_{DOC}, the doubling of R_{C_T} allows 96% of the added C_T to remain in the ocean (approximately three fourths remains in the Arctic and approximately one fourth is found in the Atlantic after 70 years of simulation). Out of the C_T that remains in the Arctic Ocean, 71% ends up in the central Arctic Ocean, while the remainder is distributed between the CAA (10%), the Barents Sea (6%), the Laptev Sea (5%), the Kara Sea (4%), the East Siberian Sea (3%), and the Chukchi and Beaufort Seas (1% each). Only 4% of that additional C_T is emitted to the atmosphere (Table 5) because R_{A_T} is assumed to increase exactly in step with R_{C_T}. Therefore, the $R^{\star}_{A_T}$:$R^{\star}_{C_T}$ (equation (1)) ratio increases in RIC while it decreases in ROC.

For simplicity, the PISCES model assumes that R_{A_T} equals R_{C_T}. In contrast, in three out of the five major Arctic rivers that drain directly into the Arctic Ocean, the A_T:C_T ratio varies from 0.91 to 0.94 (Tank, Raymond, et al. 2012). In the remaining two major Arctic rivers, the Kolyma and Ob, that ratio is 0.7 and 0.84, respectively. Thus, in the RIC simulation, the amount of added C_T that is not buffered by an equivalent increase in A_T, is up to 30%, a fraction that behaves as does the pure C_T added in the ROC simulation where terrigenous DOC is assumed to be instantaneously remineralized to C_T at the river mouth. Thus, by assuming R_{A_T} to be equal to R_{C_T}, we underestimate the outgassing of CO_2 in RIC and overestimate the corresponding increase in pH and Ω_{arag} as detailed in the following section.

4.3. $R^{\star}_{A_T}$:$R^{\star}_{C_T}$ Ratio and Coastal Ocean Acidification

Doubling R_{DOC} decreases the $R^{\star}_{A_T}$: $R^{\star}_{C_T}$ flux ratio (equation (1)) from 0.71 to 0.55, i.e., for ΔROC, which in turn lowers the Arctic coastal ocean A_T:C_T ratio along with pH and Ω_{arag}. Basinwide average changes of pH and Ω_{arag} both reach −0.02, at most 7% of the respective changes due to the atmospheric CO_2 increase

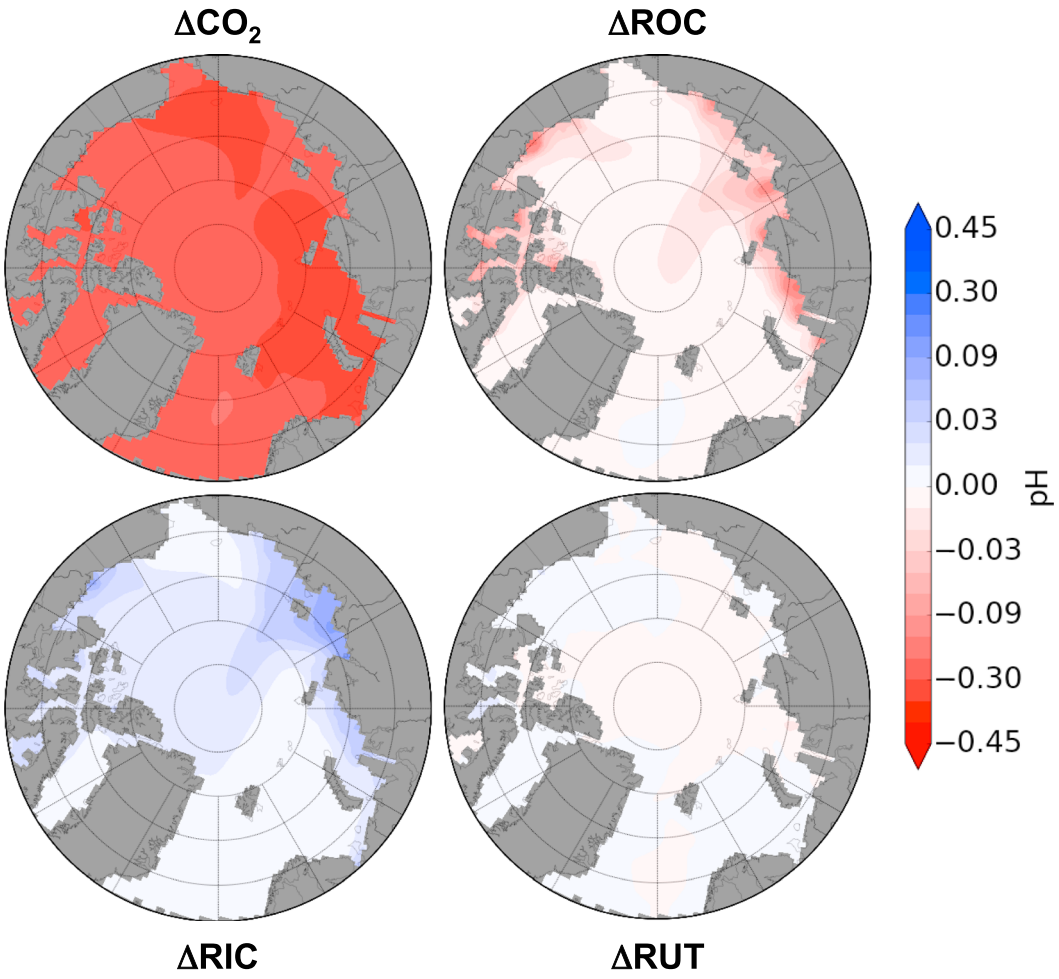

Figure 5. Modeled changes in pH for ΔCO_2, ΔROC, ΔRIC, and ΔRUT.

(Table 6). Larger changes occur in the regional seas, for example, reaching up to −0.08 for pH and −0.09 for Ω_{arag}, at most 30% of the respective changes due to the atmospheric CO_2 increase. The largest simulated changes occur very near to river mouths and are up to 3–37 times larger than surrounding regional averages (Figure 5), as they decline sharply with distance away from each river mouth while the added C_T (from R_{DOC}) is mostly lost via CO_2 outgassing (section 4.2). Thus, doubling R_{DOC} mainly affects the waters very close to river mouths, where local CO_2 outgassing nearly reaches levels seen for basinwide average ingassing from the doubling of atmospheric CO_2 (Figure 5). In the model, there is also some signature of low pH and low Ω_{arag} along the transpolar drift (Figures 5 and 6) from offshore transport of coastal waters into the central Arctic Ocean.

Contrary to case for R_{DOC}, doubling the model's R_{C_T} comes along with an equal, simultaneous increase in $R^{\star}_{A_T}$ by definition. Thus, doubling R_{C_T} increases the $R^{\star}_{A_T}$: $R^{\star}_{C_T}$ ratio from 0.55 to 0.71 because R_{DOC} is nonzero (equation (1)) and in the model that is instantly converted to a flux of C_T only. Furthermore, this increase in the $R^{\star}_{A_T}$: $R^{\star}_{C_T}$ ratio leads to an increase in the ocean A_T:C_T ratio. Hence, there are increases in the Arctic Ocean's surface average pH (0.02) and Ω_{arag} (0.06) (Table 6). The largest simulated regional average pH increases from doubling of R_{C_T} occur in the Laptev Sea (0.06) and Beaufort Sea (0.04). There that doubling cancels 21% and 15% of the corresponding pH declines from the atmospheric CO_2 doubling, based on our idealized assumption that atmospheric CO_2, R_{C_T}, and R_{DOC} all increase at the same rate. The largest changes in surface pH occur near river mouths and are 2 to 3 times larger than surrounding regional changes, a smaller factor than for the case of R_{DOC} doubling where river mouth maxima were 3–37 times larger than corresponding regional changes. These lower river mouth coastal sea gradients from the doubling of R_{C_T}

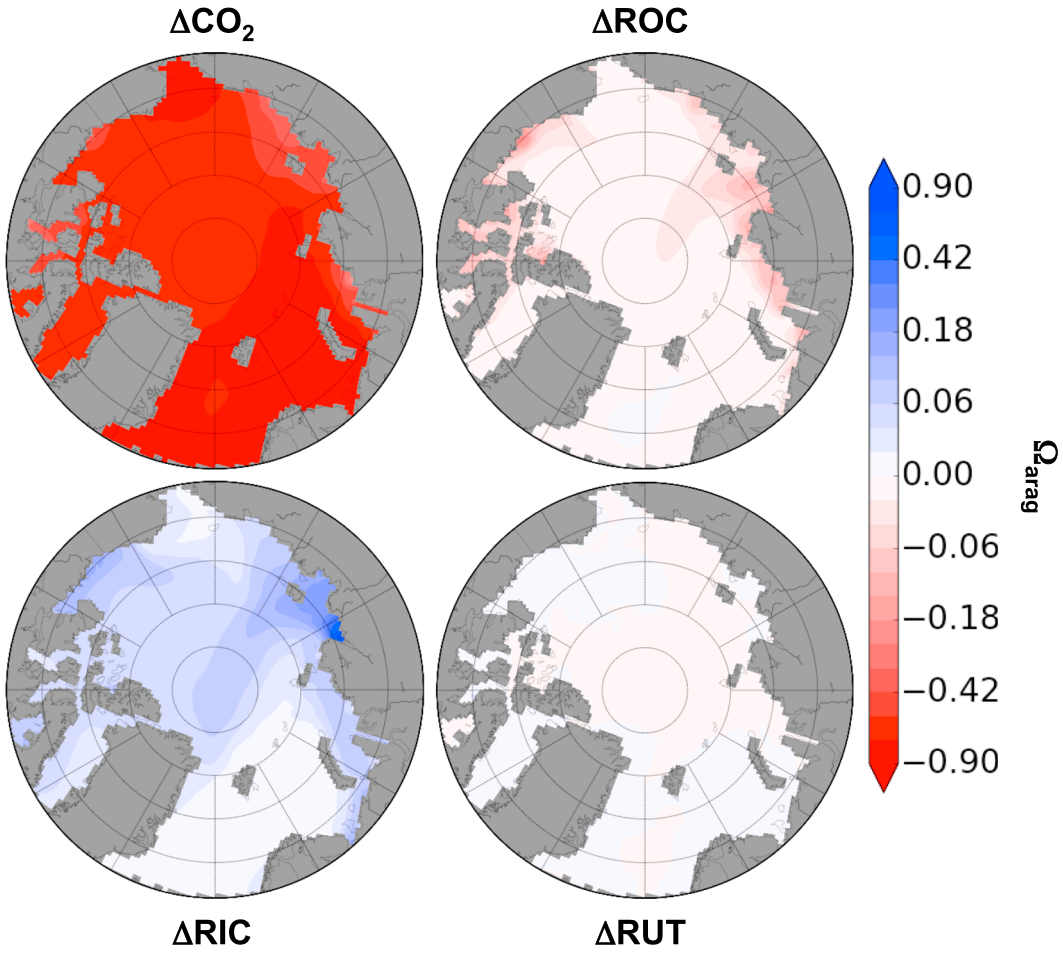

Figure 6. Modeled changes in Ω_{arag} for ΔCO2, ΔROC, ΔRIC, and ΔRUT.

are attributed to the lack of CO_2 outgassing from increasing R_{C_T} and the transport of the additional C_T and A_T from rivers away from river mouths.

Regarding simulated Ω_{arag}, its largest regional changes from the doubling of R_{C_T} occur in the Laptev Sea (0.19) and Beaufort Sea (0.11; Table 6), both regions with relatively higher R_{C_T} to R_{DOC} ratios (Table 1). Those increases in those two seas offset 35% and 19% of the declines from doubling of atmospheric CO_2. As seen for pH, the maximal changes of Ω_{arag} occur very near river mouths and are 2 to 3 times larger than surrounding regional changes.

However, our results are subject to two simplifications concerning riverine fluxes: the instantaneous conversion of terrigenous DOC to C_T and R_{A_T}:R_{C_T}=1. These two simplifications partly compensate one another, as the comparison between our $R^{\star}_{A_T}$:$R^{\star}_{C_T}$ ratio and a reconstructed $R^{\star}_{A_T}$:$R^{\star}_{C_T}$ ratio based on more realistic cases (R_{DOC} lability of 50%, and R_{A_T}:R_{C_T} as in Tank, Raymond, et al., 2012) suggest (Figure S1). The two simplifications also cause the temporal change of the $R^{\star}_{A_T}$:$R^{\star}_{C_T}$ ratio in the ROC and RIC simulations to be 26–55% larger than the more realistic cases in four out of five major Arctic rivers. Only for the Ob River do the two simplifications lead to a reduction (by 7%) of the change in $R^{\star}_{A_T}$:$R^{\star}_{C_T}$ from the doubling of R_{DOC} and R_{C_T}. Basinwide then, our estimates of the effects of doubling R_{DOC} and R_{C_T} on pH and Ω_{arag} are likely overestimated.

5. Sensitivity Factors

The sensitivity factors evolve over time but tend to stabilize by year 70 (Figures S2–S5). Sensitivity factors for carbon storage (ζ) take longer to stabilize because the timescale for penetration of anthropogenic carbon

Table 7
Mean Arctic Ocean Sensitivities of Carbon Storage (ζ), Air-to-Sea CO_2 Flux (β), NPP (η), and pH (ξ) to Changes in Atmospheric CO_2, R_{DOC}, R_{C_T}, and R_{NUT} as Defined in Section 2.5 and Integrated Changes Over Years 0–70

	Sensitivity		Integrated change	
		Carbon storage		
$\zeta_{\Delta CO_2}$	22.27	Tg C ppm^{-1}	6.38	Pg C
$\zeta_{\Delta ROC}$	0.05	Tg C (Tg C)$^{-1}$	0.03	Pg C
$\zeta_{\Delta RIC}$	0.71	Tg C (Tg C)$^{-1}$	1.12	Pg C
$\zeta_{\Delta RUT}$	0.58	Tg C (Tg N)$^{-1}$	0.04	Pg C
		Air-to-sea CO_2		
$\beta_{\Delta CO_2}$	4.82	Tg C ppm^{-1}	1.38	Pg C
$\beta_{\Delta ROC}$	−0.86	Tg C (Tg C)$^{-1}$	−0.55	Pg C
$\beta_{\Delta RIC}$	−0.05	Tg C (Tg C)$^{-1}$	−0.07	Pg C
$\beta_{\Delta RUT}$	2.29	Tg C (Tg N)$^{-1}$	0.17	Pg C
		Net primary production		
$\eta_{\Delta RUT}$	1.07	Tg N (Tg N)$^{-1}$	0.08	Pg N
		pH		
$\xi_{\Delta CO_2}$	−0.001	ppm^{-1}	−0.30	
$\xi_{\Delta ROC}$	−0.029	(Pg C)$^{-1}$	−0.02	
$\xi_{\Delta RIC}$	0.011	(Pg C)$^{-1}$	0.02	

Note. NPP = net primary production.

into the deep ocean is much longer than our 70-year simulation, unlike for the shorter timescales of the other sensitivity factors, which are tied to the surface.

These sensitivity factors for air-to-sea CO_2 flux (β), ocean carbon storage (ζ), NPP (η), and surface pH (ξ) are summarized as time-integrated values at year 70 when forcing variables are doubled. Our simulated sensitivity of global ocean anthropogenic carbon uptake to increasing atmospheric CO_2 ($\beta^{global}_{\Delta CO_2}$) may be compared to estimates from an ensemble of CMIP5 models forced under a 1%/year atmospheric CO_2 increase scenario (Arora et al., 2013). Our $\beta^{global}_{\Delta CO_2}$ of 0.9 Pg C/ppm lies at the upper limit of the CMIP5 model range (0.7–0.9 Pg C/ppm). The model sensitivity for the Arctic Ocean alone ($\beta_{\Delta CO_2}$) is 4.8 Tg C/ppm, only 0.5% of the analogous global sensitivity $\beta^{global}_{\Delta CO_2}$ even though the Arctic Ocean surface comprises 4% of the global ocean surface area. The relatively low $\beta_{\Delta CO_2}$ for the Arctic Ocean is consistent with the regional distribution of the CMIP5 results (Ciais et al., 2013, Figure 6.22), which show a lower air-to-sea flux sensitivity to increasing atmospheric CO_2 for the Arctic Ocean compared to global values. In contrast, the sensitivity for Arctic Ocean carbon storage $\zeta_{\Delta CO_2}$ (22.3 Tg C/ppm) is 2% of the corresponding global sensitivity, although the Arctic Ocean contains only 1% of the global ocean's water volume. That 2:1 ratio is consistent with that seen for the data-based estimates of anthropogenic carbon storage in the Arctic Ocean (Tanhua et al., 2009). The difference between the Arctic $\beta_{\Delta CO_2}$ and $\zeta_{\Delta CO_2}$ confirms that most of today's anthropogenic carbon stored in the Arctic Ocean is imported from the Atlantic and Pacific (Terhaar et al., 2019a).

In a consistent fashion, we calculated the sensitivity of the air-to-sea CO_2 flux and carbon storage to changes in riverine carbon input. The sensitivity of the air-to-sea CO_2 flux to changes in R_{DOC} ($\beta_{\Delta ROC}$) is −0.86 Tg C (Tg C)$^{-1}$, indicating that 86% of additional C_T from R_{DOC} has been lost by CO_2 outgassing (Table 7). Conversely with the increase in R_{C_T}, only 5% of the additional C_T is lost to the atmosphere ($\beta_{\Delta RIC} = -0.05$ Tg C (Tg C)$^{-1}$). In terms of Arctic Ocean carbon storage, increasing R_{DOC} enhances that by 0.05 Tg C for every teragram of carbon of R_{DOC} that is added to the ocean as C_T. This low regional $\zeta_{\Delta ROC}$ is in line with the corresponding largely negative $\beta_{\Delta ROC}$, which is consistent with most of the added C_T from the increase in R_{DOC} being lost to the atmosphere. Conversely, the Arctic's $\zeta_{\Delta RIC}$ of 0.71 Tg C (Tg C)$^{-1}$ is 14 times larger than its $\zeta_{\Delta ROC}$ (Table 7), highlighting that most of the additional C_T from R_{C_T} remains in the ocean since there is an equal increase in $R^{\star}_{A_T}$ and hence surface ocean pCO_2 is hardly affected (section 4.2). For both ΔROC and ΔRIC, the sum of the absolute numbers of β and ζ is below 1, indicating that after 70 years, the remainder

(difference relative to 1.0) has left the Arctic Ocean laterally to the North Atlantic, that is, 0.09 Tg C (Tg C)$^{-1}$ for ΔROC and 0.24 Tg C (Tg C)$^{-1}$ for ΔRIC.

Likewise, we are interested in the sensitivities of NPP, the air-to-sea CO_2 flux, and ocean carbon storage to riverine nutrient input. The increase in Arctic Ocean NPP from the increase in the riverine nitrogen flux is $\eta_{\Delta RUT} = 1.07$ Tg N (Tg N)$^{-1}$ (Table 7), that is, more than is fueled from Arctic rivers alone. That extra Arctic NPP may be fueled in part by additional river nutrients added from outside the Arctic, given that R_{NUT} is increased in all rivers globally and assuming there is sufficient transport from adjacent regions. It could also come in part from the remineralization of the additional organic matter produced by the increases in R_{NUT}, for example, on the Arctic shelf. The increase in NPP also drives increases in the Arctic Ocean air-to-sea CO_2 flux ($\beta_{\Delta RUT} = 2.29$ Tg C (Tg N)$^{-1}$) and carbon storage ($\zeta_{\Delta RUT} = 0.58$ Tg C (Tg N)$^{-1}$). The difference between $\beta_{\Delta RUT}$ and $\zeta_{\Delta RUT}$ can be explained by lateral export to the Atlantic Ocean and the enhanced storage of carbon in organic matter and POC by enhanced NPP. Based on the model's C:N molar ratio of 122:16, an additional carbon uptake of 6.99 Tg C (Tg N)$^{-1}$ would have been expected if every mole of carbon consumed by NPP would have been replaced via the air-to-sea CO_2 flux. Yet, the simulated $\beta_{\Delta RUT}$ reveals that only 33% of the C_T removed by NPP is replaced via invasion of atmospheric CO_2. This result is consistent with an earlier estimate of air-to-sea CO_2 flux enhancement from NPP by Orr and Sarmiento (1992) for the global ocean (43%), although here the focus is on the Arctic Ocean with its large shelf seas and high riverine inputs.

Lastly, sensitivities of surface ocean pH were assessed with respect to increases in atmospheric CO_2, R_{DOC}, and R_{C_T}. The sensitivity of Arctic surface pH to the increase in R_{DOC} ($\xi_{\Delta ROC}$) is −0.029 (Pg C)$^{-1}$. Increasing R_{C_T} along with $R^{\star}_{A_T}$ leads to an increase in pH by 0.011 (Pg C)$^{-1}$ ($\xi_{\Delta RIC}$) because the simultaneous and equal increases in R_{C_T} and $R^{\star}_{A_T}$ increase the $R^{\star}_{A_T} : R^{\star}_{C_T}$ ratio (equation (1)). Relative to these basinwide average sensitivities, locally sensitivities can be several times larger, for example, near river mouths (sections 4.1–4.3).

When integrated over the 70-year simulation, carbon storage from the doubling of riverine R_{DIC} fluxes amounts to 18% of carbon storage from the doubling of atmospheric CO_2 (Table 7). In comparison, carbon storage from the doubling of riverine R_{DOC} and R_{NUT} fluxes each amount to 0.5% of carbon storage from the doubling of atmospheric CO_2. In terms of the air-to-sea CO_2 flux, the doubling of R_{DOC} causes an outgassing that amounts to 40% of the magnitude of the ingassing from the doubling of atmospheric CO_2, while the doubling of R_{DIC} has the same opposing effect but amounts to only 5%. Conversely, the doubling of R_{NUT} increased the simulated air-to-sea CO_2 flux by an amount that is equivalent to 12% of that from the doubling of atmospheric CO_2. Changes in mean surface pH from the doubling of riverine R_{DOC} and R_{DIC} fluxes each amount to 7% of the change from the doubling of atmospheric CO_2.

6. Conclusions

This study offers a preliminary assessment of the extent to which certain key biogeochemical characteristics of the Arctic Ocean are sensitive to changes in river fluxes of carbon and nutrients. It provides a quantitative view that helps to disentangle how these characteristics are affected across the Arctic Ocean by riverine inputs of terrigenous organic carbon, inorganic carbon, and nutrients. Doubling the riverine nutrient flux increases Arctic NPP by 11% on average, by more than 30% in the Laptev and Beaufort Seas, and by up to 100% near river mouths. Doubling riverine DOC fluxes enhances ocean CO_2 outgassing, nearly offsetting the influx of anthropogenic CO_2 through the Arctic Ocean's air-sea interface from an imposed simultaneous doubling of atmospheric CO_2. However, much more anthropogenic carbon enters the Arctic Ocean laterally. Doubling riverine DOC fluxes also reduces the $R^{\star}_{A_T}$:$R^{\star}_{C_T}$ ratio, thus enhancing ocean acidification. Average changes in surface pH and Ω_{arag} due to the doubling of riverine DOC fluxes amount to at most 7% of the changes due to the doubling of atmospheric CO_2, while that proportion reaches up to 30% in regional seas and up to 100% close to river mouths. Conversely, doubling river C_T fluxes increases the $R^{\star}_{A_T}$: $R^{\star}_{C_T}$ ratio and thus reduces ocean acidification. That reduction is at most 8% of the opposite effect from the doubling of atmospheric CO_2 in terms of the basinwide average, but it amounts to up to 21% of regional sea averages and up to 50% near river mouths.

This study takes a first step toward assessing the influence of changing riverine input on Arctic Ocean biogeochemistry. The approach is limited by model simplifications, for example, its relatively coarse lateral resolution (1°), which does not explicitly resolve mesoscale and submesoscale processes (Holt et al., 2008). Beyond eddies, coastal upwelling and internal tides are poorly represented (Holt et al., 2014; Nurser & Bacon,

2014). Such weaknesses also affect simulated ocean biogeochemistry (Holt et al., 2008), for example, the air-to-sea CO_2 flux (Bianchi et al., 2005). Future work with nested models could potentially alleviate these physical concerns while limiting the computational investment.

These results suggest that the effects of riverine DOC fluxes should also be considered in the debate about whether the Arctic Ocean will become a source or a sink of CO_2 (Bates & Mathis, 2009; Cai et al., 2010; Manizza et al., 2019; Roy et al., 2011). Likewise, riverine nutrient fluxes should be accounted for in another debate, the one about how nutrient supply to the surface Arctic Ocean will change and whether those changes will enhance or reduce NPP in the future (Arrigo & van Dijken, 2015; Cai et al., 2010; Vancoppenolle et al., 2013). Indeed, the wide divergence between NPP projections among the CMIP5 models (Vancoppenolle et al., 2013) may be partly due to the lack of accounting of riverine nutrient fluxes in some models. Not accounting for the effects of riverine carbon fluxes may also lead to biased projections of pH and Ω_{arag} in Arctic shelf seas. Our finding that doubling riverine C_T fluxes reduces coastal ocean acidification is counterintuitive if one does not consider the implicit simultaneous increase in A_T. Although this finding is based on two simplifications, more realistic assumptions still lead to a future increase in $R^{\star}_{A_T}$:$R^{\star}_{C_T}$ and hence reduced acidification from an increase in riverine inorganic carbon delivery.

Overall, our results suggest that even in the Arctic Ocean, where riverine inputs are proportionally the largest, the effects of decadal-to-centennial changes in river fluxes of carbon and nutrients on open ocean biogeochemistry are relatively small. Yet they also suggest that for coastal seas, the influence of riverine input of carbon and nutrients should not be neglected, as often is the case in ocean models.

Acknowledgments
We thank C. Nangini and L. Kwiatkowski for comments. This study was funded through the EU H2020 project C-CASCADES (Marie Sklodowska-Curie grant 643052). Support is also acknowledged for J. C. O. from the French ANR project SOBUMS (ANR-16-CE01-0014), for L. B. from the H2020 CRESCENDO grant (641816) and the MTES/FRB Acidoscope project, and for P. R. from the H2020 VERIFY grant (776810). Simulations were made using HPC resources from the French GENCI-IDRIS program (grant x2015010040). Model output was stored and analyzed on the CICLAD platform at the IPSL. The code for the NEMO ocean model version 3.2 is available under CeCILL license online (http://www.nemo-ocean.eu). Data (model output) are available online (https://doi.org/10.17882/59399; Terhaar et al., 2019b).

References

Anderson, L. G., Jutterström, S., Hjalmarsson, S., Wåhlström, I., & Semiletov, I. P. (2009). Outgassing of CO_2 from Siberian Shelf seas by terrestrial organic matter decomposition. *Geophysical Research Letters*, *36*, L20601. https://doi.org/10.1029/2009GL040046

Anderson, L. G., & Kaltin, S. (2001). Carbon fluxes in the Arctic Ocean—Potential impact by climate change. *Polar Research*, *20*(2), 225–232. https://doi.org/10.3402/polar.v20i2.6521

Anderson, L. G., Tanhua, T., Björk, G., Hjalmarsson, S., Jones, E. P., Jutterström, S., et al. (2010). Arctic ocean shelf-basin interaction: An active continental shelf CO_2 pump and its impact on the degree of calcium carbonate solubility. *Deep Sea Research Part I*, *57*(7), 869–879. https://doi.org/10.1016/j.dsr.2010.03.012

Arora, V. K., Boer, G. J., Friedlingstein, P., Eby, M., Jones, C. D., Christian, J. R., et al. (2013). Carbon-concentration and carbon-climate feedbacks in CMIP5 Earth system models. *Journal of Climate*, *26*(15), 5289–5314. https://doi.org/10.1175/JCLI-D-12-00494.1

Arrigo, K. R., Pabi, S., van Dijken, G. L., & Maslowski, W. (2010). Air-sea flux of CO_2 in the Arctic Ocean, 1998-2003. *Journal of Geophysical Research*, *115*, G04024. https://doi.org/10.1029/2009JG001224

Arrigo, K. R., & van Dijken, G. L. (2011). Secular trends in Arctic Ocean net primary production. *Journal of Geophysical Research*, *116*, C09011. https://doi.org/10.1029/2011JC007151

Arrigo, K. R., & van Dijken, G. L. (2015). Continued increases in Arctic Ocean primary production. *Progress in Oceanography*, *136*, 60–70. https://doi.org/10.1016/j.pocean.2015.05.002

Aumont, O., Ethé, C., Tagliabue, A., Bopp, L., & Gehlen, M. (2015). PISCES-v2: An ocean biogeochemical model for carbon and ecosystem studies. *Geoscientific Model Development*, *8*(8), 2465–2513. https://doi.org/10.5194/gmd-8-2465-2015

Barnier, B., Madec, G., Penduff, T., Molines, J.-M., Treguier, A.-M., Le Sommer, J., et al. (2006). Impact of partial steps and momentum advection schemes in a global ocean circulation model at eddy-permitting resolution. *Ocean Dynamics*, *56*(5-6), 543–567. https://doi.org/10.1007/s10236-006-0082-1

Bates, N., & Mathis, J. (2009). The Arctic Ocean marine carbon cycle: Evaluation of air-sea CO_2 exchanges, ocean acidification impacts and potential feedbacks. *Biogeosciences*, *6*(11), 2433–2459. https://doi.org/10.5194/bg-6-2433-2009

Bates, N. R., Moran, S. B., Hansell, D. A., & Mathis, J. T. (2006). An increasing CO_2 sink in the Arctic Ocean due to sea-ice loss. *Geophysical Research Letters*, *33*, L23609. https://doi.org/10.1029/2006GL027028

Bianchi, A. A., Bianucci, L., Piola, A. R., Pino, D. R., Schloss, I., Poisson, A., & Balestrini, C. F. (2005). Vertical stratification and air-sea CO_2 fluxes in the Patagonian shelf. *Journal of Geophysical Research*, *110*, C07003. https://doi.org/10.1029/2004JC002488

Boer, G. J., & Arora, V. (2010). Geographic aspects of temperature and concentration feedbacks in the carbon budget. *Journal of Climate*, *23*(3), 775–784. https://doi.org/10.1175/2009JCLI3161.1

Bourgeois, T., Orr, J. C., Resplandy, L., Terhaar, J., Ethé, C., Gehlen, M., & Bopp, L. (2016). Coastal-ocean uptake of anthropogenic carbon. *Biogeosciences*, *13*(14), 4167–4185. https://doi.org/10.5194/bg-13-4167-2016

Brodeau, L., Barnier, B., Treguier, A.-M., Penduff, T., & Gulev, S. (2010). An ERA40-based atmospheric forcing for global ocean circulation models. *Ocean Modelling*, *31*(3), 88–104. https://doi.org/10.1016/j.ocemod.2009.10.005

Cai, W.-J. (2003). Riverine inorganic carbon flux and rate of biological uptake in the Mississippi River plume. *Geophysical Research Letters*, *30*(2), 1032. https://doi.org/10.1029/2002GL016312

Cai, W.-J., Chen, L., Chen, B., Gao, Z., Lee, S. H., Chen, J., et al. (2010). Decrease in the CO_2 uptake capacity in an ice-free Arctic Ocean basin. *Science*, *329*(5991), 556–559. https://doi.org/10.1126/science.1189338

Carmack, E. C., Yamamoto-Kawai, M., Haine, T. W. N., Bacon, S., Bluhm, B. A., Lique, C., et al. (2015). Freshwater and its role in the Arctic Marine System: Sources, disposition, storage, export, and physical and biogeochemical consequences in the Arctic and global oceans. *Journal of Geophysical Research: Biogeosciences*, *121*, 675–717. https://doi.org/10.1002/2015JG003140

Chierici, M., & Fransson, A. (2009). Calcium carbonate saturation in the surface water of the Arctic Ocean: Undersaturation in freshwater influenced shelves. *Biogeosciences*, *6*(11), 2421–2431. https://doi.org/10.5194/bg-6-2421-2009

Ciais, P., Sabine, C., Bala, G., Bopp, L., Brovkin, V., Canadell, J., et al. (2013). Carbon and other biogeochemical cycles. In T. Stocker, D. Qin, G.-K. Plattner, M. Tignor, S. Allen, J. Boschung, et al. (Eds.), *Climate change 2013: The physical science basis. Contribution of working group I to the fifth assessment report of the intergovernmental panel on climate change* (pp. 465–570). Cambridge, United Kingdom and New York, NY, USA: Cambridge University Press. https://doi.org/10.1017/CBO9781107415324.015

Dai, A., & Trenberth, K. E. (2002). Estimates of freshwater discharge from continents: Latitudinal and seasonal variations. *Journal of Hydrometeorology*, *3*(6), 660–687. https://doi.org/10.1175/1525-7541(2002)003<0660:EOFDFC>2.0.CO;2

Darnis, G., Robert, D., Pomerleau, C., Link, H., Archambault, P., Nelson, R. J., et al. (2012). Current state and trends in Canadian Arctic marine ecosystems: II. Heterotrophic food web, pelagic-benthic coupling, and biodiversity. *Climatic Change*, *115*(1), 179–205. https://doi.org/10.1007/s10584-012-0483-8

Dee, D. P., Uppala, S. M., Simmons, A. J., Berrisford, P., Poli, P., Kobayashi, S., et al. (2011). The ERA-Interim reanalysis: Configuration and performance of the data assimilation system. *Quarterly Journal of the Royal Meteorological Society*, *137*(656), 553–597. https://doi.org/10.1002/qj.828

Déry, S. J., Hernández-Henríquez, M. A., Burford, J. E., & Wood, E. F. (2009). Observational evidence of an intensifying hydrological cycle in northern Canada. *Geophysical Research Letters*, *36*, L13402. https://doi.org/10.1029/2009GL038852

Déry, S. J., & Wood, E. F. (2005). Decreasing river discharge in northern Canada. *Geophysical Research Letters*, *32*, L10401. https://doi.org/10.1029/2005GL022845

Drake, T. W., Tank, S. E., Zhulidov, A. V., Holmes, R. M., Gurtovaya, T., & Spencer, R. G. M. (2018). Increasing alkalinity export from large Russian Arctic rivers. *Environmental Science & Technology*, *52*(15), 8302–8308. https://doi.org/10.1021/acs.est.8b01051

Frey, K. E., & McClelland, J. W. (2008). Impacts of permafrost degradation on Arctic river biogeochemistry. *Hydrological Processes*, *23*(1), 169–182. https://doi.org/10.1002/hyp.7196

Frey, K. E., McClelland, J. W., Holmes, R. M., & Smith, L. C. (2007). Impacts of climate warming and permafrost thaw on the riverine transport of nitrogen and phosphorus to the Kara Sea. *Journal of Geophysical Research*, *112*, G04S58. https://doi.org/10.1029/2006JG000369

Frey, K. E., & Smith, L. C. (2005). Amplified carbon release from vast West Siberian peatlands by 2100. *Geophysical Research Letters*, *32*, L09401. https://doi.org/10.1029/2004GL022025

Friedlingstein, P., Bopp, L., Ciais, P., Dufresne, J.-L., Fairhead, L., LeTreut, H., et al. (2001). Positive feedback between future climate change and the carbon cycle. *Geophysical Research Letters*, *28*, 1543–1546. https://doi.org/10.1029/2000GL012015

Friedlingstein, P., Cox, P., Betts, R., Bopp, L., von Bloh, W., Brovkin, V., et al. (2006). Climate-carbon cycle feedback analysis: Results from the CMIP4 model intercomparison. *Journal of Climate*, *19*(14), 3337–3353. https://doi.org/10.1175/JCLI3800.1

Friedlingstein, P., Dufresne, J. L., Cox, P. M., & Rayner, P. (2003). How positive is the feedback between climate change and the carbon cycle? *Tellus B*, *55*(2), 692–700. https://doi.org/10.3402/tellusb.v55i2.16765

Gent, P. R., & McWilliams, J. C. (1990). Isopycnal mixing in ocean circulation models. *Journal of Physical Oceanography*, *20*(1), 150–155. https://doi.org/10.1175/1520-0485(1990)020<0150:IMIOCM>2.0.CO;2

Hansell, D. A., Kadko, D., & Bates, N. R. (2004). Degradation of terrigenous dissolved organic carbon in the western Arctic Ocean. *Science*, *304*(5672), 858–861. https://doi.org/10.1126/science.1096175

Harsch, M. A., Hulme, P. E., McGlone, M. S., & Duncan, R. P. (2009). Are treelines advancing? A global meta-analysis of treeline response to climate warming. *Ecology Letters*, *12*(10), 1040–1049. https://doi.org/10.1111/j.1461-0248.2009.01355.x

Hill, V. J., Matrai, P. A., Olson, E., Suttles, S., Steele, M., Codispoti, L., & Zimmerman, R. C. (2013). Synthesis of integrated primary production in the Arctic Ocean: II. In situ and remotely sensed estimates. *Progress in Oceanography*, *110*, 107–125. https://doi.org/10.1016/j.pocean.2012.11.005

Holmes, R. M., McClelland, J. W., Peterson, B. J., Tank, S. E., Bulygina, E., Eglinton, T. I., et al. (2012). Seasonal and annual fluxes of nutrients and organic matter from large rivers to the Arctic Ocean and surrounding seas. *Estuaries Coasts*, *35*(2), 369–382. https://doi.org/10.1007/s12237-011-9386-6

Holmes, R. M., McClelland, J. W., Raymond, P. A., Frazer, B. B., Peterson, B. J., & Stieglitz, M. (2008). Lability of DOC transported by Alaskan rivers to the Arctic Ocean. *Geophysical Research Letters*, *35*, L03402. https://doi.org/10.1029/2007GL032837

Holmes, R. M., Peterson, B. J., Gordeev, V. V., Zhulidov, A. V., Meybeck, M., Lammers, R. B., & Vörösmarty, C. J. (2000). Flux of nutrients from Russian rivers to the Arctic Ocean: Can we establish a baseline against which to judge future changes? *Water Resources Research*, *36*(8), 2309–2320. https://doi.org/10.1029/2000WR900099

Holmes, R., Peterson, B., Zhulidov, A., Gordeev, V., Makkaveev, P., Stunzhas, P., et al. (2001). Nutrient chemistry of the Ob' and Yenisey Rivers, Siberia: Results from June 2000 expedition and evaluation of long-term data sets. *Marine Chemistry*, *75*(3), 219–227. https://doi.org/10.1016/S0304-4203(01)00038-X

Holt, J., Allen, J. I., Anderson, T. R., Brewin, R., Butenschön, M., Harle, J., et al. (2014). Challenges in integrative approaches to modelling the marine ecosystems of the North Atlantic: Physics to fish and coasts to ocean. *Progress in Oceanography*, *129*, 285–313. https://doi.org/10.1016/j.pocean.2014.04.024

Holt, J., Harle, J., Proctor, R., Michel, S., Ashworth, M., Batstone, C., et al. (2008). Modelling the global coastal ocean. *Philosophical Transactions of the Royal Society A*, *367*(1890), 939–951.

Jakobsson, M. (2002). Hypsometry and volume of the Arctic Ocean and its constituent seas. *Geochemistry, Geophysics, Geosystems*, *3*(5), 1–18. https://doi.org/10.1029/2001GC000302

Jakobsson, M., Cherkis, N., Woodward, J., Macnab, R., & Coakley, B. (2000). New grid of Arctic bathymetry aids scientists and mapmakers. *Eos, Transactions American Geophysical Union*, *81*(9), 89–96. https://doi.org/10.1029/00EO00059

Joesoef, A., Kirchman, D. L., Sommerfield, C. K., & Cai, W.-J. (2017). Seasonal variability of the inorganic carbon system in a large coastal plain estuary. *Biogeosciences*, *14*(21), 4949–4963. https://doi.org/10.5194/bg-14-4949-2017

Kaiser, K., Benner, R., & Amon, R. M. W. (2017). The fate of terrigenous dissolved organic carbon on the Eurasian shelves and export to the North Atlantic. *Journal of Geophysical Research: Oceans*, *122*, 4–22. https://doi.org/10.1002/2016JC012380

Körtzinger, A., Hedges, J. I., & Quay, P. D. (2001). Redfield ratios revisited: Removing the biasing effect of anthropogenic CO_2. *Limnology and Oceanography*, *46*(4), 964–970. https://doi.org/10.4319/lo.2001.46.4.0964

Lauvset, S. K., Key, R. M., & Perez, F. F. (2016). A new global interior ocean mapped climatology: The $1^\circ \times 1^\circ$ GLODAP version 2. *Earth System Science Data*, *8*(2), 325. https://doi.org/10.5194/essd-8-325-2016

Lawrence, D. M., & Slater, A. G. (2005). A projection of severe near-surface permafrost degradation during the 21^{st} century. *Geophysical Research Letters*, *32*, L24401. https://doi.org/10.1029/2005GL025080

Le Fouest, V., Babin, M., & Tremblay, J.-E. (2013). The fate of riverine nutrients on Arctic shelves. *Biogeosciences*, *10*(6), 3661–3677. https://doi.org/10.5194/bg-10-3661-2013

Le Fouest, V., Manizza, M., Tremblay, B., & Babin, M. (2015). Modelling the impact of riverine DON removal by marine bacterioplankton on primary production in the Arctic Ocean. *Biogeosciences*, *12*(11), 3385–3402. https://doi.org/10.5194/bg-12-3385-2015

Le Fouest, V., Matsuoka, A., Manizza, M., Shernetsky, M., Tremblay, B., & Babin, M. (2018). Towards an assessment of riverine dissolved organic carbon in surface waters of the western Arctic Ocean based on remote sensing and biogeochemical modeling. *Biogeosciences*, *15*(5), 1335–1346. https://doi.org/10.5194/bg-15-1335-2018

Letscher, R. T., Hansell, D. A., & Kadko, D. (2011). Rapid removal of terrigenous dissolved organic carbon over the Eurasian shelves of the Arctic Ocean. *Marine Chemistry*, *123*(1), 78–87. https://doi.org/10.1016/j.marchem.2010.10.002

Letscher, R. T., Hansell, D. A., Kadko, D., & Bates, N. R. (2013). Dissolved organic nitrogen dynamics in the Arctic Ocean. *Marine Chemistry*, *148*, 1–9. https://doi.org/10.1016/j.marchem.2012.10.002

Ludwig, W., Amiotte-Suchet, P., Munhoven, G., & Probst, J.-L. (1998). Atmospheric CO_2 consumption by continental erosion: Present-day controls and implications for the last glacial maximum. *Global and Planetary Change*, *16*, 107–120. https://doi.org/10.1016/S0921-8181(98)00016-2

Lythe, M. B., & Vaughan, D. G. (2001). BEDMAP: A new ice thickness and subglacial topographic model of Antarctica. *Journal of Geophysical Research*, *106*(B6), 11,335–11,351. https://doi.org/10.1029/2000JB900449

Madec, G. (2008). *NEMO ocean engine*. France: Note du Pôle de modélisation, Institut Pierre-Simon Laplace (IPSL). No 27, ISSN No 1288-1619.

Madec, G., & Imbard, M. (1996). A global ocean mesh to overcome the North Pole singularity. *Climate Dynamics*, *12*(6), 381–388. https://doi.org/10.1007/BF00211684

Manizza, M., Follows, M. J., Dutkiewicz, S., McClelland, J. W., Menemenlis, D., Hill, C. N., et al. (2009). Modeling transport and fate of riverine dissolved organic carbon in the Arctic Ocean. *Global Biogeochemical Cycles*, *23*, GB4006. https://doi.org/10.1029/2008GB003396

Manizza, M., Follows, M. J., Dutkiewicz, S., Menemenlis, D., McClelland, J. W., Hill, C. N., et al. (2011). A model of the Arctic Ocean carbon cycle. *Journal of Geophysical Research*, *116*, C12020. https://doi.org/10.1029/2011JC006998

Manizza, M., Menemenlis, D., Miller, E. C., & Zhang, H. (2019). Modeling the recent changes in the Arctic Ocean CO_2 sink (2006–2013). *Global Biogeochemical Cycles*, *33*, 420–438. https://doi.org/10.1029/2018GB006070

Mann, P. J., Eglinton, T. I., McIntyre, C. P., Zimov, N., Davydova, A., Vonk, J. E., et al. (2015). Utilization of ancient permafrost carbon in headwaters of Arctic fluvial networks. *Nature Communications*, *6*, 7856. https://doi.org/10.1038/ncomms8856

Mathis, J. T., Cross, J. N., & Bates, N. R. (2011). Coupling primary production and terrestrial runoff to ocean acidification and carbonate mineral suppression in the eastern Bering Sea. *Journal of Geophysical Research*, *116*, C02030. https://doi.org/10.1029/2010JC006453

Matsuoka, A., Hill, V., Huot, Y., Babin, M., & Bricaud, A. (2011). Seasonal variability in the light absorption properties of western arctic waters: Parameterization of the individual components of absorption for ocean color applications. *Journal of Geophysical Research*, *116*, C02007. https://doi.org/10.1029/2009JC005594

Mayorga, E., Seitzinger, S. P., Harrison, J. A., Dumont, E., Beusen, A. H., Bouwman, A., et al. (2010). Global Nutrient Export from WaterSheds 2 (NEWS 2): Model development and implementation. *Environmental Modelling & Software*, *25*(7), 837–853. https://doi.org/10.1016/j.envsoft.2010.01.007

McClelland, J. W., Déry, S. J., Peterson, B. J., Holmes, R. M., & Wood, E. F. (2006). A pan-Arctic evaluation of changes in river discharge during the latter half of the 20th century. *Geophysical Research Letters*, *33*, L06715. https://doi.org/10.1029/2006GL025753

McClelland, J. W., Holmes, R. M., Dunton, K. H., & Macdonald, R. W. (2012). The Arctic Ocean estuary. *Estuaries Coasts*, *35*(2), 353–368. https://doi.org/10.1007/s12237-010-9357-3

McClelland, J. W., Holmes, R. M., Peterson, B. J., Amon, R., Brabets, T., Cooper, L., et al. (2008). Development of a pan–Arctic database for river chemistry. *Eos, Transactions American Geophysical Union*, *89*(24), 217–218. https://doi.org/10.1029/2008EO240001

McClelland, J. W., Holmes, R. M., Peterson, B. J., & Stieglitz, M. (2004). Increasing river discharge in the Eurasian Arctic: Consideration of dams, permafrost thaw, and fires as potential agents of change. *Journal of Geophysical Research*, *109*, D18102. https://doi.org/10.1029/2004JD004583

Nohara, D., Kitoh, A., Hosaka, M., & Oki, T. (2006). Impact of climate change on river discharge projected by multimodel ensemble. *Journal of Hydrometeorology*, *7*(5), 1076–1089. https://doi.org/10.1175/JHM531.1

Nurser, A. J. G., & Bacon, S. (2014). The Rossby radius in the Arctic Ocean. *Ocean Science*, *10*(6), 967–975. https://doi.org/10.5194/os-10-967-2014

Oelke, C., Zhang, T., & Serreze, M. C. (2004). Modeling evidence for recent warming of the Arctic soil thermal regime. *Geophysical Research Letters*, *31*, L07208. https://doi.org/10.1029/2003GL019300

Olsen, A., Anderson, L. G., & Heinze, C. (2015). Arctic carbon cycle: Patterns, impacts and possible changes. In B. Evengård, J. Nymand Larsen, & Ø. Paasche (Eds.), *The new Arctic* (pp. 95–115). Cham: Springer International Publishing. https://doi.org/10.1007/978-3-319-17602-4_8

Orr, J. C., & Epitalon, J.-M. (2015). Improved routines to model the ocean carbonate system: mocsy 2.0. *Geoscientific Model Development*, *8*(3), 485–499. https://doi.org/10.5194/gmd-8-485-2015

Orr, J. C., & Sarmiento, J. L. (1992). Potential of marine macroalgae as a sink for CO_2: Constraints from a 3-D general circulation model of the global ocean. *Water, Air, & Soil Pollution*, *64*(1), 405–421. https://doi.org/10.1007/BF00477113

Peterson, B. J., Holmes, R. M., McClelland, J. W., Vörösmarty, C. J., Lammers, R. B., Shiklomanov, A. I., et al. (2002). Increasing river discharge to the Arctic Ocean. *Science*, *298*(5601), 2171–2173. https://doi.org/10.1126/science.1077445

Popova, E., Yool, A., Aksenov, Y., & Coward, A. (2013). Role of advection in Arctic Ocean lower trophic dynamics: A modeling perspective. *Journal of Geophysical Research: Oceans*, *118*, 1571–1586. https://doi.org/10.1002/jgrc.20126

Raymond, P. A., McClelland, J. W., Holmes, R. M., Zhulidov, A. V., Mull, K., Peterson, B. J., et al. (2007). Flux and age of dissolved organic carbon exported to the Arctic Ocean: A carbon isotopic study of the five largest arctic rivers. *Global Biogeochemical Cycles*, *21*, GB4011. https://doi.org/10.1029/2007GB002934

Regnier, P., Friedlingstein, P., Ciais, P., Mackenzie, F. T., Gruber, N., Janssens, I. A., et al. (2013). Anthropogenic perturbation of the carbon fluxes from land to ocean. *Nature Geoscience*, *6*(8), 597–607.

Riebesell, U., Gattuso, J.-P., Thingstad, T. F., & Middelburg, J. J. (2013). Preface "Arctic ocean acidification: Pelagic ecosystem and biogeochemical responses during a mesocosm study". *Biogeosciences*, *10*(8), 5619–5626. https://doi.org/10.5194/bg-10-5619-2013

Rousset, C., Vancoppenolle, M., Madec, G., Fichefet, T., Flavoni, S., Barthélemy, A., et al. (2015). The Louvain-La-Neuve sea ice model LIM3.6: Global and regional capabilities. *Geoscientific Model Development*, *8*(10), 2991–3005. https://doi.org/10.5194/gmd-8-2991-2015

Roy, T., Bopp, L., Gehlen, M., Schneider, B., Cadule, P., Frölicher, T. L., et al. (2011). Regional impacts of climate change and atmospheric CO_2 on future ocean carbon uptake: A multimodel linear feedback analysis. *Journal of Climate*, *24*(9), 2300–2318. https://doi.org/10.1175/2010JCLI3787.1

Semiletov, I., Pipko, I., Gustafsson, Ö., Anderson, L. G., Sergienko, V., Pugach, S., et al. (2016). Acidification of East Siberian Arctic Shelf waters through addition of freshwater and terrestrial carbon. *Nature Geoscience*, *9*(5), 361–365. https://doi.org/10.1038/ngeo2695

Smith, W. H., & Sandwell, D. T. (1997). Global sea floor topography from satellite altimetry and ship depth soundings. *Science*, *277*(5334), 1956–1962. https://doi.org/10.1126/science.277.5334.1956

Spencer, R. G. M., Aiken, G. R., Butler, K. D., Dornblaser, M. M., Striegl, R. G., & Hernes, P. J. (2009). Utilizing chromophoric dissolved organic matter measurements to derive export and reactivity of dissolved organic carbon exported to the Arctic Ocean: A case study of the Yukon River, Alaska. *Geophysical Research Letters*, *36*, L060401. https://doi.org/10.1029/2008GL036831

Steinacher, M., Joos, F., Frolicher, T. L., Plattner, G.-K., & Doney, S. C. (2009). Imminent ocean acidification in the Arctic projected with the NCAR global coupled carbon cycle-climate model. *Biogeosciences*, *6*(4), 515–533. https://doi.org/10.5194/bg-6-515-2009

Steiner, N. S., Christian, J. R., Six, K. D., Yamamoto, A., & Yamamoto-Kawai, M. (2013). Future ocean acidification in the Canada Basin and surrounding Arctic Ocean from CMIP5 earth system models. *Journal of Geophysical Research: Oceans*, *119*, 332–347. https://doi.org/10.1002/2013JC009069

Takahashi, T., Broecker, W. S., & Langer, S. (1985). Redfield ratio based on chemical data from isopycnal surfaces. *Journal of Geophysical Research*, *90*(C4), 6907–6924. https://doi.org/10.1029/JC090iC04p06907

Tanhua, T., Jones, E. P., Jeansson, E., Jutterström, S., Smethie, W. M., Wallace, D. W., & Anderson, L. G. (2009). Ventilation of the Arctic Ocean: Mean ages and inventories of anthropogenic CO_2 and CFC-11. *Journal of Geophysical Research*, *114*, C01002. https://doi.org/10.1029/2008JC004868

Tank, S. E., Frey, K. E., Striegl, R. G., Raymond, P. A., Holmes, R. M., McClelland, J. W., & Peterson, B. J. (2012). Landscape-level controls on dissolved carbon flux from diverse catchments of the circumboreal. *Global Biogeochemical Cycles*, *26*, GB0E02. https://doi.org/10.1029/2012GB004299

Tank, S. E., Manizza, M., Holmes, R. M., & Peterson, J. W. M. B. J. (2012). The processing and impact of dissolved riverine nitrogen in the Arctic Ocean. *Estuaries and Coasts*, *35*(2), 401–415. https://doi.org/10.1007/s12237-011-9417-3

Tank, S. E., Raymond, P. A., Striegl, R. G., McClelland, J. W., Holmes, R. M., Fiske, G. J., & Peterson, B. J. (2012). A land-to-ocean perspective on the magnitude, source and implication of DIC flux from major Arctic rivers to the Arctic Ocean. *Global Biogeochemical Cycles*, *26*, GB4018. https://doi.org/10.1029/2011GB004192

Terhaar, J., Orr, J. C., Gehlen, M., Ethé, C., & Bopp, L. (2019a). Model constraints on the anthropogenic carbon budget of the Arctic Ocean. *Biogeosciences*, *16*(11), 2343–2367. https://doi.org/10.5194/bg-16-2343-2019

Terhaar, J., Orr, J. C., Gehlen, M., Ethé, C., & Bopp, L. (2019b). Arctic Ocean sensitivity tests to doubling of riverine carbon and nutrient delivery simulated by the NEMO-PISCES model. SEANOE, https://doi.org/10.17882/59399

Tremblay, J.-E., Anderson, L. G., Matrai, P., Coupel, P., Bélanger, S., Michel, C., & Reigstad, M. (2015). Global and regional drivers of nutrient supply, primary production and CO_2 drawdown in the changing Arctic Ocean. *Progress in Oceanography*, *139*, 171–196. https://doi.org/10.1016/j.pocean.2015.08.009

Uotila, P., Iovino, D., Vancoppenolle, M., Lensu, M., & Rousset, C. (2017). Comparing sea ice, hydrography and circulation between NEMO3.6 LIM3 and LIM2. *Geoscientific Model Development*, *10*(2), 1009–1031. https://doi.org/10.5194/gmd-10-1009-2017

Uppala, S. M., Kållberg, P. W., Simmons, A. J., Andrae, U., Bechtold, V. D. C., Fiorino, M., et al. (2005). The ERA-40 re-analysis. *Quarterly Journal of the Royal Meteorological Society*, *131*(612), 2961–3012. https://doi.org/10.1256/qj.04.176

Vancoppenolle, M., Bopp, L., Madec, G., Dunne, J., Ilyina, T., Halloran, P. R., & Steiner, N. (2013). Future Arctic Ocean primary productivity from CMIP5 simulations: Uncertain outcome, but consistent mechanisms. *Global Biogeochemical Cycles*, *27*, 605–619. https://doi.org/10.1002/gbc.20055

Vonk, J. E., Mann, P. J., Davydov, S., Davydova, A., Spencer, R. G. M., Schade, J., et al. (2013). High biolability of ancient permafrost carbon upon thaw. *Geophysical Research Letters*, *40*, 2689–2693. https://doi.org/10.1002/grl.50348

Walvoord, M. A., & Striegl, R. G. (2007). Increased groundwater to stream discharge from permafrost thawing in the Yukon River basin: Potential impacts on lateral export of carbon and nitrogen. *Geophysical Research Letters*, *34*, L12402. https://doi.org/10.1029/2007GL030216

Wang, Z. A., Bienvenu, D. J., Mann, P. J., Hoering, K. A., Poulsen, J. R., Spencer, R. G. M., & Holmes, R. M. (2013). Inorganic carbon speciation and fluxes in the Congo River. *Geophysical Research Letters*, *40*, 511–516. https://doi.org/10.1002/grl.50160

Yasunaka, S., Murata, A., Watanabe, E., Chierici, M., Fransson, A., van Heuven, S., et al. (2016). Mapping of the air–sea CO_2 flux in the Arctic Ocean and its adjacent seas: Basin-wide distribution and seasonal to interannual variability. *Polar Science*, *10*(3), 323–334. https://doi.org/10.1016/j.polar.2016.03.006